Geophys. J. Int. (2001) **146,** 504–530

Seismic tomography shows that upwelling beneath Iceland is confined to the upper mantle

G. R. Foulger,[1] M. J. Pritchard,[1] B. R. Julian,[2] J. R. Evans,[2] R. M. Allen,[3] G. Nolet,[3] W. J. Morgan,[3] B. H. Bergsson,[4] P. Erlendsson,[4] S. Jakobsdottir,[4] S. Ragnarsson,[4] R. Stefansson[4] and K. Vogfjörd[5]

[1] *Department of Geological Sciences, University of Durham, Durham,* DH1 3LE, *UK. E-mail: G.R.Foulger@durham.ac.uk*
[2] *US Geological Survey,* 345 *Middlefield Road., Menlo Park,* CA 94025, *USA*
[3] *Department of Geological and Geophysical Sciences, Guyot Hall, Princeton University, Princeton,* NJ 08544–5807, *USA*
[4] *Meteorological Office of Iceland, Bustadavegi* 9, *Reykjavik, Iceland*
[5] *National Energy Authority, Grensasvegi* 9, *Reykjavik, Iceland*

Accepted 2001 April 3. Received 2001 March 19; in original form 2000 August 1

SUMMARY

We report the results of the highest-resolution teleseismic tomography study yet performed of the upper mantle beneath Iceland. The experiment used data gathered by the Iceland Hotspot Project, which operated a 35-station network of continuously recording, digital, broad-band seismometers over all of Iceland 1996–1998. The structure of the upper mantle was determined using the ACH damped least-squares method and involved 42 stations, 3159 *P*-wave, and 1338 *S*-wave arrival times, including the phases *P*, *pP*, *sP*, *PP*, *SP*, *PcP*, *PKIKP*, *pPKIKP*, *S*, *sS*, *SS*, *SKS* and *Sdiff*. Artefacts, both perceptual and parametric, were minimized by well-tested smoothing techniques involving layer thinning and offset-and-averaging. Resolution is good beneath most of Iceland from $\sim$60 km depth to a maximum of $\sim$450 km depth and beneath the Tjornes Fracture Zone and near-shore parts of the Reykjanes ridge. The results reveal a coherent, negative wave-speed anomaly with a diameter of 200–250 km and anomalies in *P*-wave speed, V_P, as strong as -2.7 per cent and in *S*-wave speed, V_S, as strong as -4.9 per cent. The anomaly extends from the surface to the limit of good resolution at $\sim$450 km depth. In the upper $\sim$250 km it is centred beneath the eastern part of the Middle Volcanic Zone, coincident with the centre of the $\sim$100 mGal Bouguer gravity low over Iceland, and a lower crustal low-velocity zone identified by receiver functions. This is probably the true centre of the Iceland hotspot. In the upper $\sim$200 km, the low-wave-speed body extends along the Reykjanes ridge but is sharply truncated beneath the Tjornes Fracture Zone. This suggests that material may flow unimpeded along the Reykjanes ridge from beneath Iceland but is blocked beneath the Tjornes Fracture Zone. The magnitudes of the V_P, V_S and V_P/V_S anomalies cannot be explained by elevated temperature alone, but favour a model of maximum temperature anomalies $<$200 K, along with up to $\sim$2 per cent of partial melt in the depth range $\sim$100–300 km beneath east-central Iceland. The anomalous body is approximately cylindrical in the top 250 km but tabular in shape at greater depth, elongated north–south and generally underlying the spreading plate boundary. Such a morphological change and its relationship to surface rift zones are predicted to occur in convective upwellings driven by basal heating, passive upwelling in response to plate separation and lateral temperature gradients. Although we cannot resolve structure deeper than $\sim$450 km, and do not detect a bottom to the anomaly, these models suggest that it extends no deeper than the mantle transition zone. Such models thus suggest a shallow origin for the Iceland hotspot rather than a deep mantle plume, and imply that the hotspot has been located on the spreading ridge in the centre of the north Atlantic for its entire history, and is not fixed relative to other Atlantic hotspots. The results are consistent with recent, regional full-thickness mantle tomography and whole-mantle tomography images that show a strong, low-wave-speed anomaly beneath the Iceland region that is confined to the upper mantle and

thus do not require a plume in the lower mantle. Seismic and geochemical observations that are interpreted as indicating a lower mantle, or core–mantle boundary origin for the North Atlantic Igneous Province and the Iceland hotspot should be re-examined to consider whether they are consistent with upper mantle processes.

Key words: hotspot, Iceland, seismic tomography, upper mantle, plume.

INTRODUCTION

Arthur Holmes was the first influential advocate of convection within the Earth, a process that later became generally accepted as the physical basis for Wegener's theory of continental drift (Holmes 1931). Very early, the convection hypothesis was accepted by German geodesists, who surmised that the rift zones of Iceland might overlie upwelling limbs and be widening, with magma rising passively to fill the space created (Bernauer 1943). It is now accepted that subducting slabs comprise the descending limbs of a convecting system, but the nature of the ascending flow at spreading ridges and hotspots, and the depths from which material rises, are still poorly understood.

Magmas at spreading ridges are thought to be of relatively shallow origin, perhaps no deeper than $\sim$100 km (e.g. Shen & Forsyth 1995). Subducted slabs, however, are known from earthquake activity and full-thickness mantle tomography to extend much deeper (Grand 1994). Spreading ridges thus appear not to involve upwellings on the same depth scale as downgoing slabs. It was originally suggested by Wilson (1963) and Morgan (1971, 1972) that hot material rises from the deep mantle to the surface of the Earth in jets or vertical, cylindrical 'plumes'. This hypothesis has gained wide acceptance, and has been invoked to explain large-scale geological and geophysical features such as large igneous provinces and geoid, topographic and geochemical anomalies. However, few observations require that magma rises in plumes from great depth. Whole-mantle tomography, for example, suggests that deep upwellings are very broad and diffuse, although the spatial resolution of those models cannot rule out narrow structures. Alternatives to the plume model that involve only relatively shallow processes have been proposed (e.g. King & Anderson 1998). The plume hypothesis is an elegant tenet that has achieved widespread acceptance, but it is unproven. It should thus not go unchallenged. Alternative models should be considered.

Seismic studies seeking mantle plumes include whole-mantle tomography, regional full-thickness mantle tomography, teleseismic tomography involving regional-scale seismic networks, and experiments focusing on specific plume markers. Tabular, high-wave-speed lithospheric slabs have been imaged beneath major subduction zones (e.g. van der Hilst *et al.* 1997; Fukao *et al.* 1992). However, negative wave-speed anomalies with the vertical, cylindrical morphology traditionally expected of plumes have not been detected. Three candidate bodies have been reported to date, one $\sim$2000 km wide arising from the core–mantle boundary beneath the South Atlantic and extending obliquely to the Earth's surface beneath East Africa, and two beneath the Pacific ocean (e.g. Ritsema *et al.* 1999; Megnin & Romanowicz 2000). However, none has a simple, traditional plume shape, width or geometry or can be explained as a thermal plume (Tackley 1998; van der Hilst & Karason 1999; Megnin & Romanowicz 2000).

For most hotspots there is no seismic evidence for a deep-seated origin. The best studied is the Iceland hotspot. Several independent, regional full-thickness mantle tomography and whole-mantle tomography studies have imaged a strong, broad, low-wave-speed upper mantle anomaly that occupies most of the north Atlantic at the latitude of Iceland (Hager & Clayton 1989; Zhou 1996; Bijwaard & Spakman 1999; Ritsema *et al.* 1999; Megnin & Romanowicz 2000; Karason & van der Hilst 2001a,b). In contrast, the lower mantle is characterized by anomalies at least an order of magnitude weaker, with poor repeatability of the details of individual features. The maximum depth of good resolution of land-based, regional seismic experiments in Iceland is limited to $\sim$450 km by the size of the island, and thus such studies can only image reliably the upper mantle above the transition zone. A strong, negative wave-speed anomaly is invariably detected. Allen *et al.* (1999) reported that the attenuation pattern of teleseismic waves passing beneath Iceland indicates a body no more than $\sim$200 km wide and with an anomaly in V_S of up to -12 per cent. This is considerably narrower and stronger than anomalies found in earlier teleseismic tomography experiments, which report bodies with diameters of 200–400 km and V_P anomalies of up to ~ -4 per cent (Tryggvason *et al.* 1983; Wolfe *et al.* 1997). Interpretations of these regional experiments did not consider alternative, non-plume hypotheses.

We report here the results of the largest teleseismic tomography study yet performed of the upper mantle beneath Iceland. Our study involves more stations and several times more arrival times than have been used before, and includes diverse seismic phases that improve resolving power. The results confirm the presence of a negative wave-speed anomaly in the upper mantle, but show additionally that its gross morphology varies with depth. The body is centred beneath east-central Iceland and is consistent with elevated temperature and partial melting. It extends beneath the Reykjanes ridge southwest of Iceland in the upper $\sim$200 km but terminates laterally at shallow depth beneath the Tjornes Fracture Zone north of Iceland. The body is roughly cylindrical in the upper $\sim$250 km, but at greater depth assumes a vertical, tabular morphology underlying and approximately parallel to the spreading plate boundary. Such a change in shape is expected near the bottom of rising, buoyant bodies, and our observations thus suggest that the negative wave-speed anomaly in the upper mantle beneath Iceland does not extend into the lower mantle (Foulger *et al.* 2000).

TECTONIC STRUCTURE OF ICELAND

Iceland has east–west and north–south dimensions of $\sim$500 and 350 km and lies on the spreading plate boundary in the north Atlantic. Over 30 spreading segments are exposed on land and comprise four major volcanic zones: the Northern, Eastern, Western and Middle Volcanic Zones (NVZ, EVZ, WVZ and MVZ; Fig. 1; Saemundsson 1979). The currently active spreading zone is represented by the NVZ, which developed at $\sim$7 Ma with the abandonment of a zone 150 km further

to the west (Saemundsson *et al.* 1980). The NVZ is linked to the offshore Kolbeinsey ridge by the ~120 km long, right-lateral Tjornes Fracture Zone (TFZ). The EVZ, a southward-propagating rift, is currently growing at the expense of the dwindling WVZ (Sigmundsson *et al.* 1994). The WVZ is connected to the offshore spreading plate boundary, the Reykjanes ridge, via the Reykjanes peninsula in southwest Iceland.

The Iceland hotspot is popularly thought, on the basis of geochemistry and volcanic production rates, to be currently centred beneath the northwest part of the Vatnajokull ice-cap (Schilling 1973; Sigvaldason *et al.* 1974). It has been suggested that the hotspot has migrated east with respect to the oceanic plate boundary at a rate of ~1 cm yr^{-1} over the last 55 Myr (Vink 1984), and that recently the spreading plate boundary in Iceland has migrated with it. However, these models are based on the assumption that the Iceland hotspot has remained fixed relative to other Atlantic hotspots. Furthermore, the shape of the edge of the Iceland plateau is consistent with the centre of volcanism having been relatively stationary with respect to the plate boundary over the last 26 Myr (Bott 1985).

DATA ACQUISITION

The objective of the Iceland Hotspot Project is to study the crust and upper mantle beneath Iceland. A network of 35 digital broad-band seismic stations was operated from June 1996 to August 1998—the largest deployment of such instruments ever in Iceland (Fig. 1). A primary objective was to perform teleseismic tomography of the highest quality practical. The greatest depth that may be imaged using this method is approximately equal to the network aperture, and we maximized this by deploying sensors from coast to coast, including one on the island of Grimsey north of Iceland. The network complemented the permanent Icelandic SIL (South Iceland Lowland) network (Stefánsson *et al.* 1993), from which data were also drawn. Particularly challenging was the deployment of station 23 at Grimsfjall, a nunatak on the caldera rim of the Grimsvotn volcano, within the Vatnajokull icecap. Bedrock is exposed there because the ground is warmed by geothermal heat from the Grimsvotn volcano. This station was deployed two months prior to, and at a distance of 5 km from, the eruption of the subglacial volcano Gjalp in September and October 1996 (Gudmundsson *et al.* 1997), and resulted in the serendipitous acquisition of an excellent seismic data set of volcanic earthquakes and tremor.

The equipment used was supplied by the IRIS–PASSCAL consortium. We used 24-bit REFTEK 72 A-08 data loggers recording a continuous data stream at 20 samples s^{-1} on 0.66–1.2 Gbyte disks. A triggered data stream was also recorded at 100 samples s^{-1} to enhance recordings of large local earthquakes. The sensors were Guralp three-component broad-band seismometers of type CMG-3T, which has a bandwidth

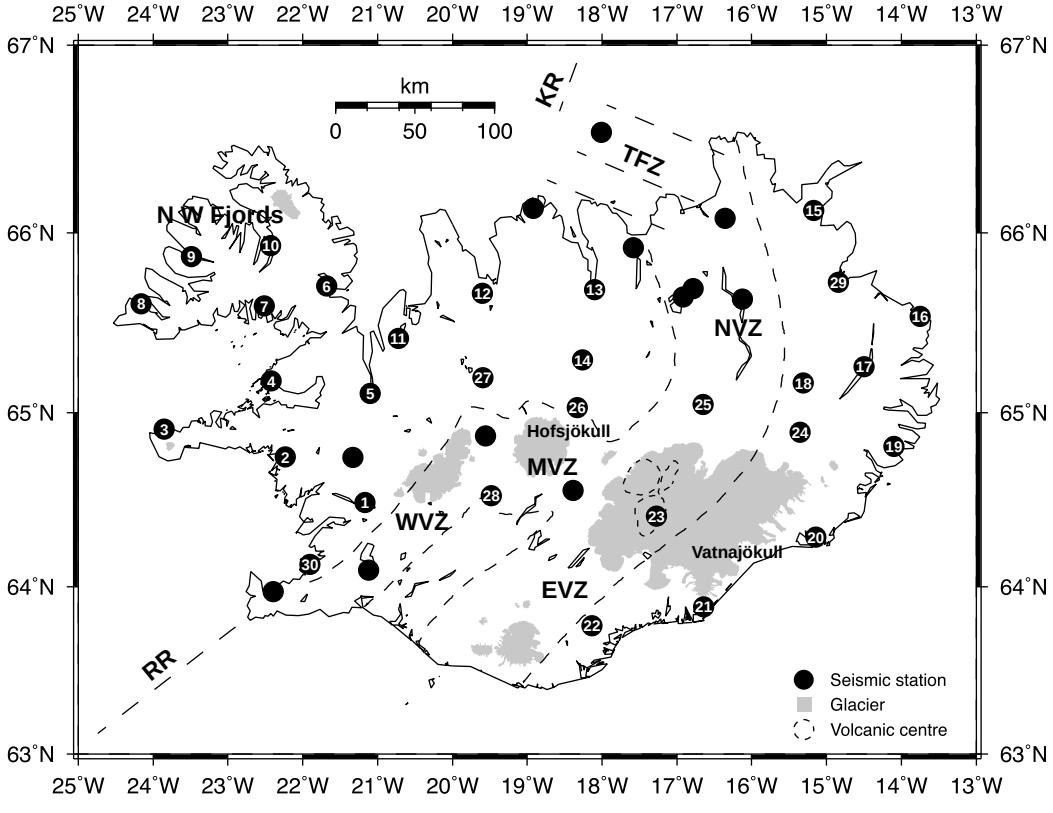

Figure 1. Map of Iceland showing the major tectonic elements. NVZ, EVZ, WVZ and MVZ: Northern, Eastern, Western and Middle Volcanic Zones; TFZ: Tjornes Fracture Zone; RR: Reykjanes ridge; KR: Kolbeinsey ridge. Grey areas: major ice-caps; black dots: broad-band seismic stations in operation 1996– 1998 that were used for this study; numbered dots: temporary stations of the Iceland Hotspot Project. Station 23 was deployed on a nunatak in the Vatnajokull ice-cap. It, along with stations 24, 25, 26 and 28, was battery-powered and deployed in mountain huts. Dots without numbers: permanent stations of the Icelandic SIL network with broad-band sensors, the five in southwest and central Iceland being supplied by the Iceland Hotspot Project.

of 0.01–50 Hz, and types CMG-3ESP and CMG-40T, which have bandwidths of 0.03–50 Hz. The CMG-40T sensors are compact and suitable for outdoors deployments where vaults have to be excavated. Microseisms are strong in Iceland, and dominated the noise compared to instrumental effects. Timing and station locations were provided by GPS clocks.

Most of the coastal zone in Iceland is populated, so we were able to deploy most of the stations in buildings, either on bedrock exposed in basements or on concrete floors laid directly onto bedrock. At these sites, mains power was used, and backup power was provided by trickle-charged batteries. Five broadband sensors were deployed in existing vaults of the Icelandic SIL network. Those data were sampled at 100 samples s^{-1} and stored in a ring buffer from which earthquakes of interest were extracted on a daily basis. The SIL data were resampled at 20 samples s^{-1} for this study. The interior of Iceland is unpopulated and not served by mains electricity, but in order to achieve uniform coverage, five stations were deployed there. We deployed the recorders in mountain huts that were selected for regularity of spacing and suitability for winter maintenance visits by a team of field workers in specially equipped snow jeeps. Winter-time power was the limiting factor at those stations, and banks of eight 150 amp hr batteries were used, trickle charged by four to eight 30 W solar panels.

All stations were visited at 6–12 week intervals. Data were dumped from field disks and archived in Reykjavik. Earthquakes were extracted on a monthly basis using event lists from the National Earthquake Information Centre (NEIC) and the Meteorological Office of Iceland, which operates the SIL network. We achieved an average of 86 per cent uptime for our stations. The most serious causes of data loss were lack of power at the interior stations, and malfunctioning of elements in outdoor excavated pits that were inaccessible throughout the winter because of frozen ground. The final data archive comprises $\sim$200 Gbytes of data compressed with the Steim algorithm (Halbert *et al.* 1988), and is publicly available over the internet from the IRIS–PASSCAL Consortium Data Management Center.

DATA PROCESSING

Teleseismic earthquake arrival times were measured on rotated seismograms using the interactive computer program DBPICK (Harvey & Quinlan 1996). The signal-to-noise ratio of seismic recordings in Iceland is degraded by microseismic and wind-generated noise, but the 2 yr deployment period was sufficient to gather excellent recordings of more than 120 teleseisms. Using preliminary arrival times computed using the IASP91 earth model (Kennett & Engdahl 1991) and NEIC final locations, traces were time-shifted to align the first-arriving *P* phase to facilitate waveform comparison. Phases picked were *P*, *pP*, *sP*, *PP*, *SP*, *PcP*, *PKIKP*, *pPKIKP*, *S*, *sS*, *SS*, *SKS* and *Sdiff*. (Table 1). For the final inversion we selected picks made in the frequency band 0.5–2.0 Hz for *P* waves and 0.05–0.1 Hz for *S* waves. We picked by hand for consistency, since initial trials with numerical cross-correlation revealed that frequent cycle misidentification occurred. Furthermore, algorithms that correlate several cycles of waveforms introduce systematic errors, since later cycles include crustal reverberations and multipathing, which vary across a large network deployed in an inhomogeneous region. Such errors may distort final models more seriously than the slightly larger but random errors in hand picks. We measured times of the first trough or peak relative to the phase of interest, with an estimated accuracy of $\sim$0.05 s for *P* phases and $\sim$0.5 s for *S* phases. Weights were assigned to picks on the basis of qualitative judgement of the clarity of the phases. Traveltime residuals were calculated by subtracting the arrival times predicted by the IASP91 model from each observed time.

Table 1. Details of phases used in the inversions.

Phase	No. earthquakes	Distance range, Δ°
P	86	30–95
pP	14	35–92
sP	2	57–58
PP	33	69–145
SP	3	94–126
PcP	2	37–58
PKIKP	12	119–142
pPKIKP	1	130
S	52	30–99
sS	4	69–92
SS	14	57–146
SKS	1	101
Sdiff	3	103–118

The surface-reflected phases *PP* and *SS* are particularly valuable because, for a given epicentral distance, they have larger slownesses than most other teleseismic body phases and can therefore help to increase vertical resolution where earthquakes at small epicentral distances are sparse, as is the case for Iceland. In particular, use of *PP* and *SS* phases can reduce vertical smearing, and help to distinguish true vertical structures from artefacts of poor resolution. The results of previous studies of mantle structure beneath Iceland are open to question, partly because of failure to use such phases (Keller *et al.* 2000). At the same time, however, surface-reflected phases introduce their own problems because their rays are not minimum-time paths. Reflections from points on the surface other than the geometrical ray bounce-point can arrive before the geometrical arrival, so signals tend to have emergent beginnings whose absolute onset times are difficult to measure. Relative arrival times must thus be measured for peaks or troughs later in the waveform, which are more subject to contamination by crustal structure variations and multipathing. In this study, we used *PP* phases from 33 earthquakes and *SS* phases from 14. To minimize the errors discussed above, we used only phases with high signal-to-noise ratios and waveforms that were coherent from station to station.

In a data set of this size, some measurements inevitably have large errors, caused, for example, by comparing different peaks or troughs at different stations, and it is important to identify and remove such outliers. This can be done by comparing the patterns of arrival-time anomalies at different stations for earthquakes with similar locations. For such a collection of events, the ray paths beneath the network are similar, and therefore, in the absence of errors, the pattern of arrival-time anomalies is also similar. We divided the phases into 10 azimuth–slowness bins for *P* and nine for *S* (Fig. 2) and analysed each bin separately. Fig. 3 shows an example of a single bin of *P* waves arriving from the east-northeast. The ordinate for each symbol gives the arrival-time anomaly minus the median value for the event for all stations. The median value plotted for each event is

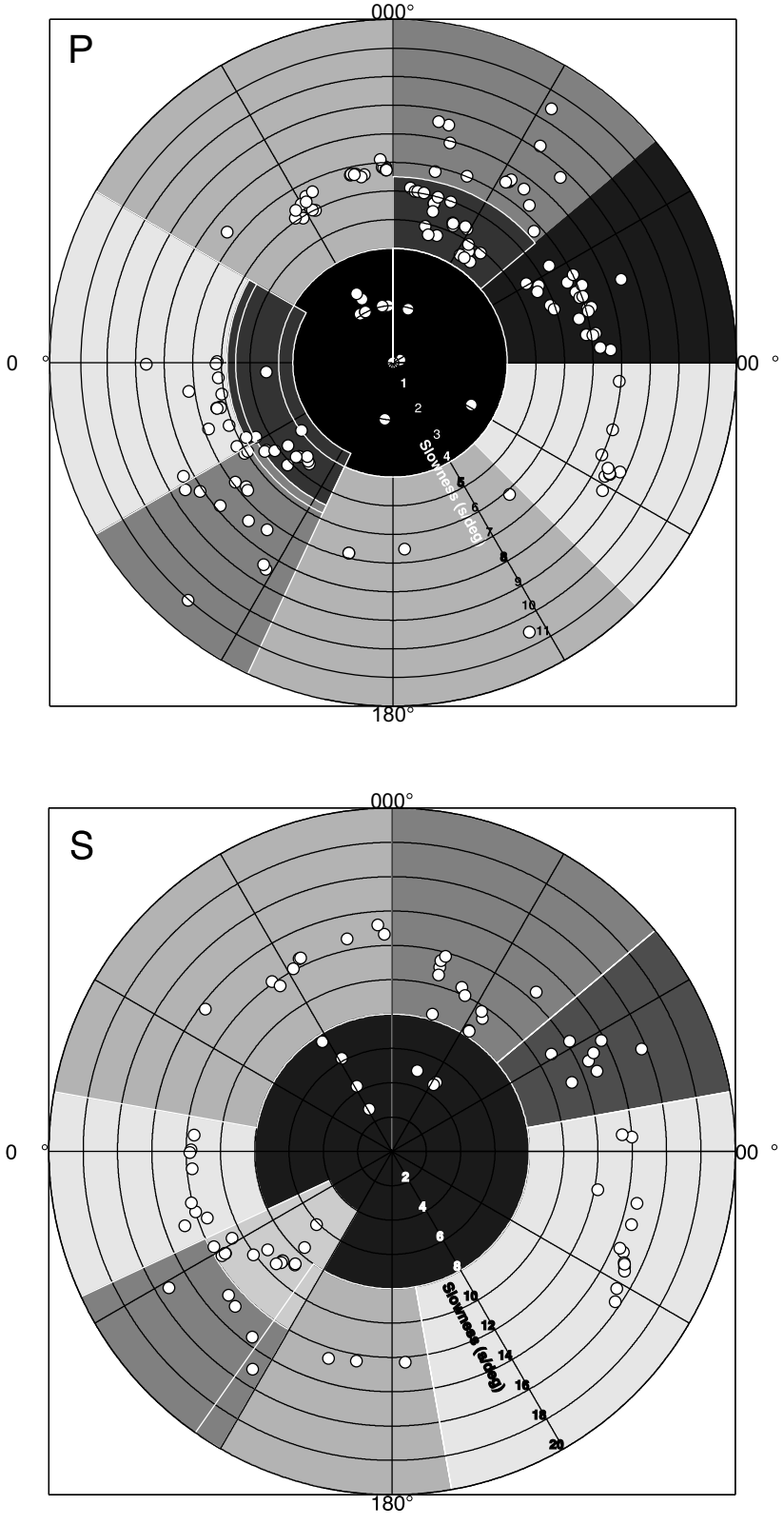

Figure 2. Azimuth–slowness bins into which phases were divided for outlier identification (Fig. 3). Double dividing lines indicate overlapping bins. Upper panel: *P* phases; lower panel: *S* phases.

thus zero. Data on plots such as this that deviated from the median value for the station by more than ± 0.6 s for *P* or ± 1.5 s for *S* were assumed to contain large errors and eliminated. The final data set contains 3159 *P* arrivals from 160 phases and 113 earthquakes, and 1338 *S* arrivals from 73 phases and 66 earthquakes (Fig. 4). The peak magnitudes of the mean arrival-time anomalies at a station were about 1 s for *P* waves and 3 s for *S* waves.

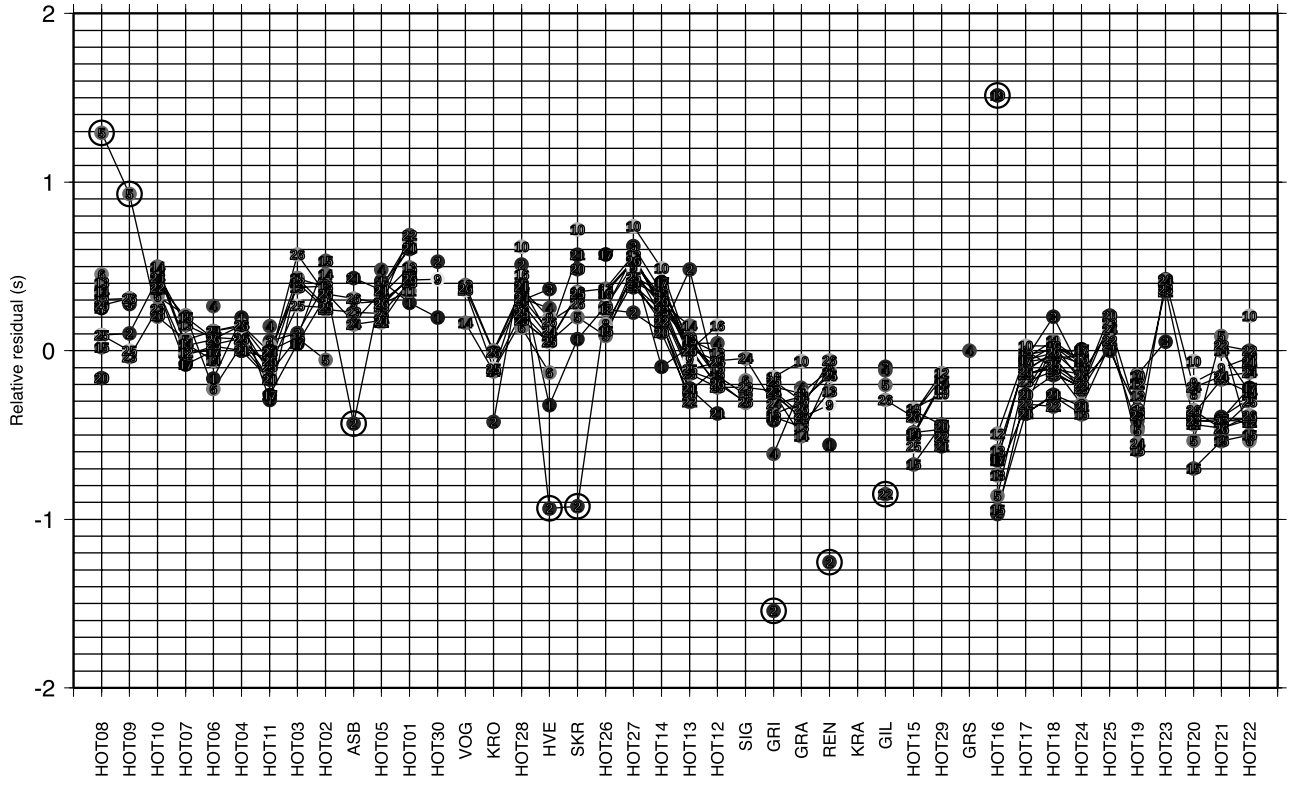

Figure 3. Example of a plot used to identify outliers, for *P* waves from events in the outer bin between ~50°E and 90°E (Fig. 2, upper panel). Each dot corresponds to an observation. Its ordinate is the arrival-time anomaly minus the median anomaly for the event. Circled dots: observations identified as outliers.

TOMOGRAPHY METHOD

To invert the arrival-time anomalies and determine 3-D structure, we used the 'ACH' damped-least-squares method of Aki *et al.* (1977). In particular, we used a version of the computer program THRD that had been modified to correct a geometrical error that is important at high latitudes (Julian *et al.* 2001). A comprehensive description of the method and application is given by Evans & Achauer (1993). The ACH method uses data from a network of seismic stations whose aperture is small compared with the distances to the sources. The 3-D structure is represented as a stack of layers, each divided into homogeneous rectangular blocks. The optimum block size depends on the station spacing. Blocks should have horizontal dimensions of approximately the average station spacing, and layers should initially have thicknesses about 1.5 times this width. The method requires that all rays enter the study volume through its base, so the model cannot extend deeper than the turning point of the shallowest incoming ray. Well-conditioned experiments involve rays distributed widely in azimuth–slowness space, and thus the study volume is a truncated cone that broadens downwards.

The ACH method perturbs an initial 1-D wave-speed model to minimize the arrival-time anomalies in the least-squares sense. Only in those places where there are many crossing rays, well distributed in azimuth and slowness, is the structure well resolved. The near surface, where there are no crossing rays, is treated differently, by solving for a single wave-speed anomaly in a cone beneath each station (a 'special first layer'). A key assumption is that delays caused by structure outside the study volume are the same for all stations for a particular event and phase. Clearly this is only an approximation, and heterogeneities outside the study volume can introduce spurious anomalies into peripheral parts of the final images (Evans & Achauer 1993). These parts must thus be viewed with caution. Furthermore, the method computes the effects of changing wave speeds in the blocks by applying Fermat's Principle to ray paths appropriate to the initial 1-D, layered structure, and thus ignores the second-order effect of refraction of rays by horizontal variations in wave speed. The severity of this approximation depends on both the magnitude of the wave-speed anomalies and their geometry. Because the rays follow minimum-time paths, regions of high wave speed are sampled most heavily, and the wave speeds in the derived models tend to be overestimated. In practice, the errors introduced have been found to be negligible if wave-speed anomalies are less than ~5 per cent (Steck & Prothero 1991), which is the case for the upper mantle beneath Iceland.

To choose optimum block sizes and damping parameters, we performed trial inversions using layers 100 km thick and blocks 100, 75 and 50 km wide (Pritchard 2000). In all cases, the homogeneous cones used to approximate variations in crustal structure beneath the stations were taken to be 10 km high. As a starting model, we used a layered approximation to the IASP91 wave-speed model. We performed a suite of inversions varying only the damping parameter, and studied the trade-off between residual variance and the square of the Euclidean length of the model vector **m**. A damping-parameter value of 400 s^2 per cent^{-2} provided a reasonable trade-off between data fit and model complexity.

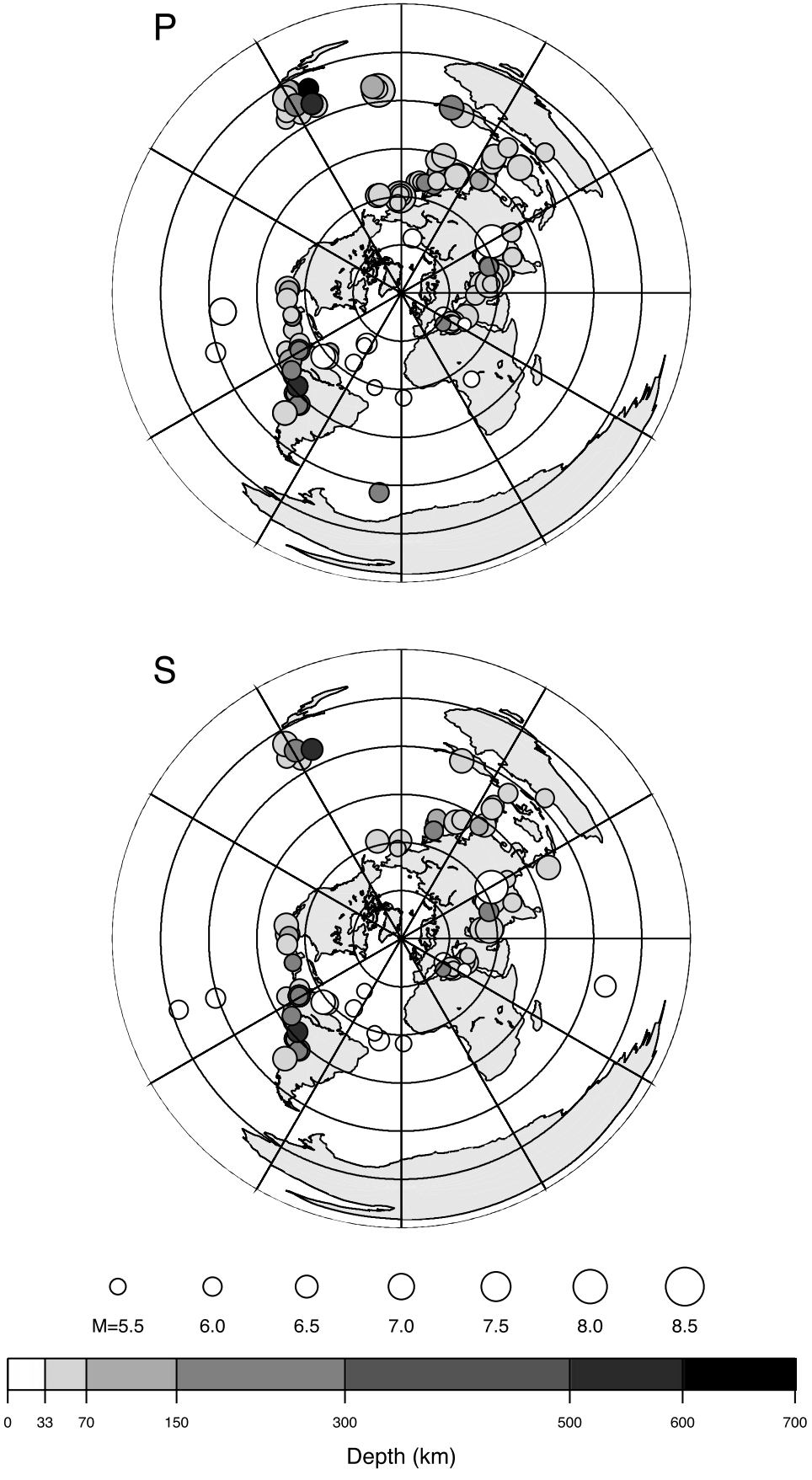

Figure 4. Azimuthal-equidistant map of the world, showing earthquakes used for the tomographic inversion. Symbol size indicates earthquake magnitude and shading indicates focal depth.

The ACH method is prone to non-linear effects that can introduce distortion into 3-D models. The effect whereby the sensitivity of the method to features smaller than the block size depends on their position with respect to the block boundaries is known as the 'disappearing anomaly' effect. An anomaly near the centre of a block can be resolved more easily than one near a block corner. We dealt with this problem by applying the 'offset-and-averaging' procedure of Evans & Achauer (1993). The original grid is offset by $1/n$ times the block size along each horizontal axis, where n is a small integer, and an additional n^2-1 offset models are computed. The final model is the average of all n^2 models. This averaging also smoothes the model horizontally.

In order to smooth the model vertically, to remove visual artefacts, we used 'layer thinning' (Evans & Achauer 1993). This procedure involves performing a final inversion with layers thinner by a factor of m, a small integer, than the initial value used (which in the case of this study was 100 km). The damping parameter must simultaneously be reduced by about a factor of m to compensate for the increased number of blocks in the model. For our layer-thinned inversions we used $m=2$ and a damping value of 225 s^2 per $cent^{-2}$. Increasing the number of blocks reduces the number of rays per block, and thus reduces formal statistical resolution. However, using synthetic tests, Evans & Achauer (1993) showed that layer thinning yields vertical smoothing without loss of ability to retrieve true Earth structure, so that the equivalent spatial resolution of the layer-thinned models is the same as that of full-thickness layer models.

We performed a suite of inversions with block widths of 100, 75 or 50 km and layer thicknesses of 100, 50 or 33 km, both with and without offset-and-averaging, for $n=2$ (Pritchard 2000). Agreement of the overall results between inversions was good for the first-order features we interpret in this paper. Pritchard (2000) showed additionally models with 100 km wide blocks and 100 km thick layers that yielded smooth, averaged structures, and models with 50 km wide blocks and 33 km thick layers that yielded noisier results. Our preferred final V_P and V_S models used offset-and-averaging with $n=2$, blocks 75 km wide and layers 50 km thick (Fig. 5), a compromise between under-modelling the data and over-modelling noise. For the original models, the initial and final rms arrival-time anomalies for P waves are 0.49 and 0.19 s, and for S waves 3.27 and 1.08 s. The 3-D models thus give data variance reductions of 84 per cent for P and 89 per cent for S. Values for the offset-and-averaged models are expected to be approximately the same.

We studied four measures of inversion quality. The hit-count (the number of rays sampling each block) is shown for P and S waves in Figs 6 and 7 for the model with 75 km wide blocks and 100 km thick layers. The whole of Iceland is well sampled from the surface down to $\sim$450 km depth. Below this, the best-sampled areas are to the north of Iceland, where blocks down to over 600 km depth are sampled by >100 P waves and >50 S waves, and to the southwest of Iceland.

Hit-count is a poor indicator of resolving power because the locations of anomalies can be determined well only if the structure is sampled by crossing rays. Arrival times measured from a bundle of quasi-parallel rays can detect the existence a wave-speed anomaly but are insensitive to its position along the ray bundle. More detailed information is provided by the resolution matrix **R** (Evans & Achauer 1993, eq. 13.18), which specifies the mapping between the 'true' Earth **m** and the inversion result $\hat{\mathbf{m}}$,

$$\hat{\mathbf{m}} = \mathbf{R}\mathbf{m}\,. \tag{1}$$

R is based on assumptions, most notably that the true Earth consists of homogeneous blocks and that ray theory accurately describes the paths of seismic waves. The diagonal elements of the resolution matrix provide relative measures of the ability of the data set to detect anomalies in different locations. Figs 8 and 9 show the diagonal elements of **R** for V_P and V_S for 75 km wide blocks and 100 km thick layers. These are good indicators of the quality of our preferred models with 50 km thick layers (Evans & Achauer 1993). The pictures are broadly similar for V_P and V_S. Resolution greater than $\sim$0.8, which exists throughout much of our models, is unusually good for studies of this kind. There is no resolution in the top $\sim$60 km of the model since there are no crossing rays there. In the depth range $\sim$60–450 km, resolution is high beneath most of Iceland except in the upper 100 km beneath a small area in south Iceland. Below 450 km, resolution decreases, and at great depth resolution is poor, the incoming rays diverge strongly and smearing is strong.

The diagonal elements of the resolution matrix do not describe the tendency of an anomaly to be imaged in the wrong location along a ray bundle, i.e. the degree of smearing. Such information is contained in the off-diagonal elements of **R**, and by examining these columns for blocks at key locations we can assess the reliability of the shapes and sizes of features of interest. A useful quantity for this purpose is the 'volume metric' of a diagonal element R_{ij} defined as the volume within which the largest positive off-diagonal elements of column i sum to some value d (Evans & Achauer 1993). Figs 10 and 11 show the 'volume metrics' of selected blocks for the final V_P and V_S models, computed for $d=0.95$, a high (pessimistic) value compared with the values of 0.5–0.7 usually used (Evans & Achauer 1993).

Smearing in the central part of the study volume is minor, and confined to a few vertically adjacent blocks. Smearing on the north, south, east and west peripheries of the study volume

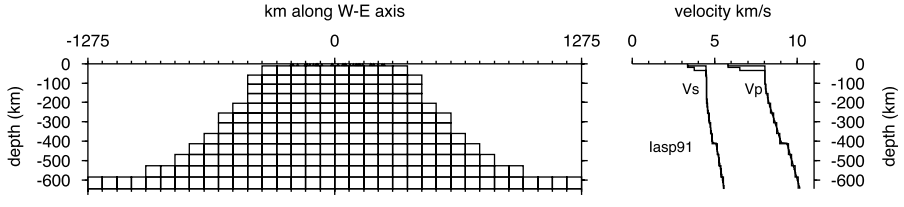

Figure 5. West–east cross-section of the block structure used for the final inversion, which uses blocks 75 km wide and layers 50 km thick. Wave-speed profiles at right show initial V_P and V_S models obtained from the IASP91 model (Kennett & Engdahl 1991).

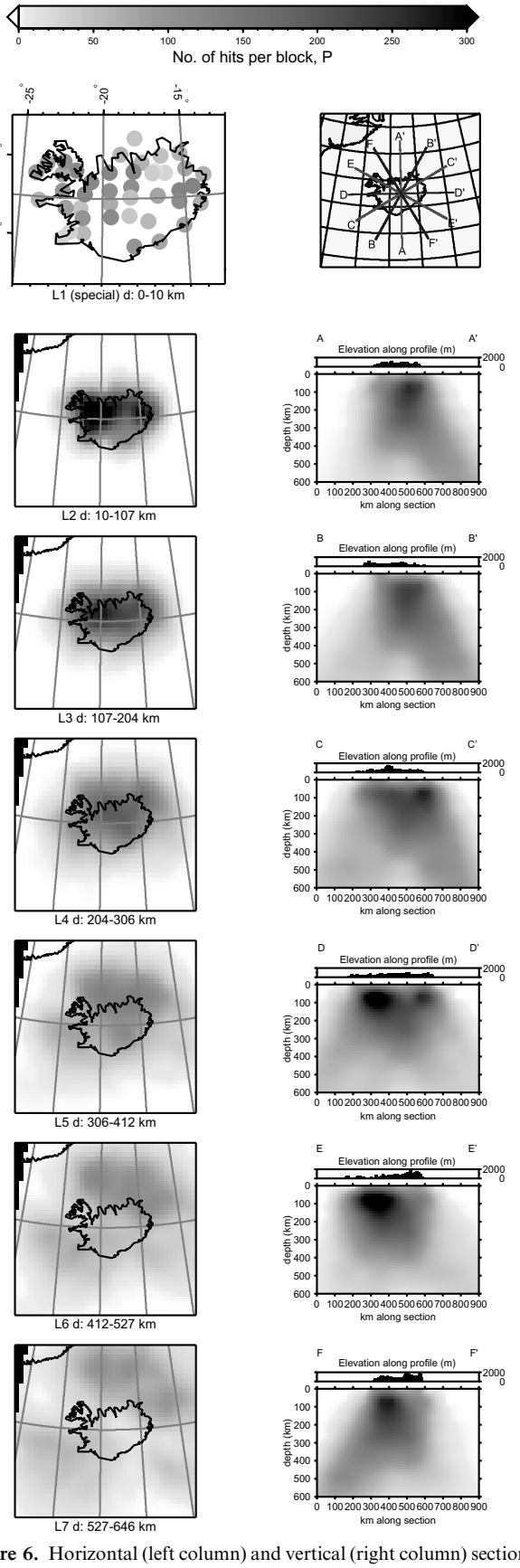

Figure 6. Horizontal (left column) and vertical (right column) sections showing the hit-count for *P* waves for the model with 75 km wide blocks and 100 km thick layers. Top left panel shows hit-counts for individual stations. Top right panel shows lines of vertical cross-sections.

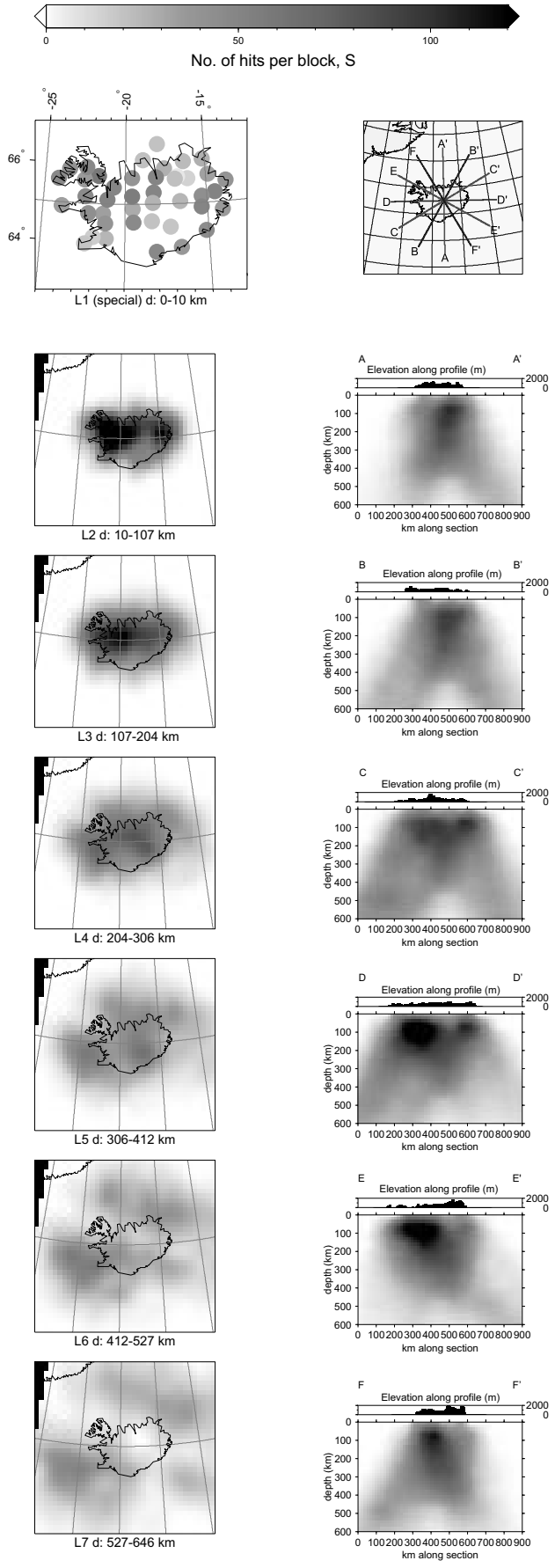

Figure 7. Same as Fig. 6 for *S* waves. Note the different greyscale.

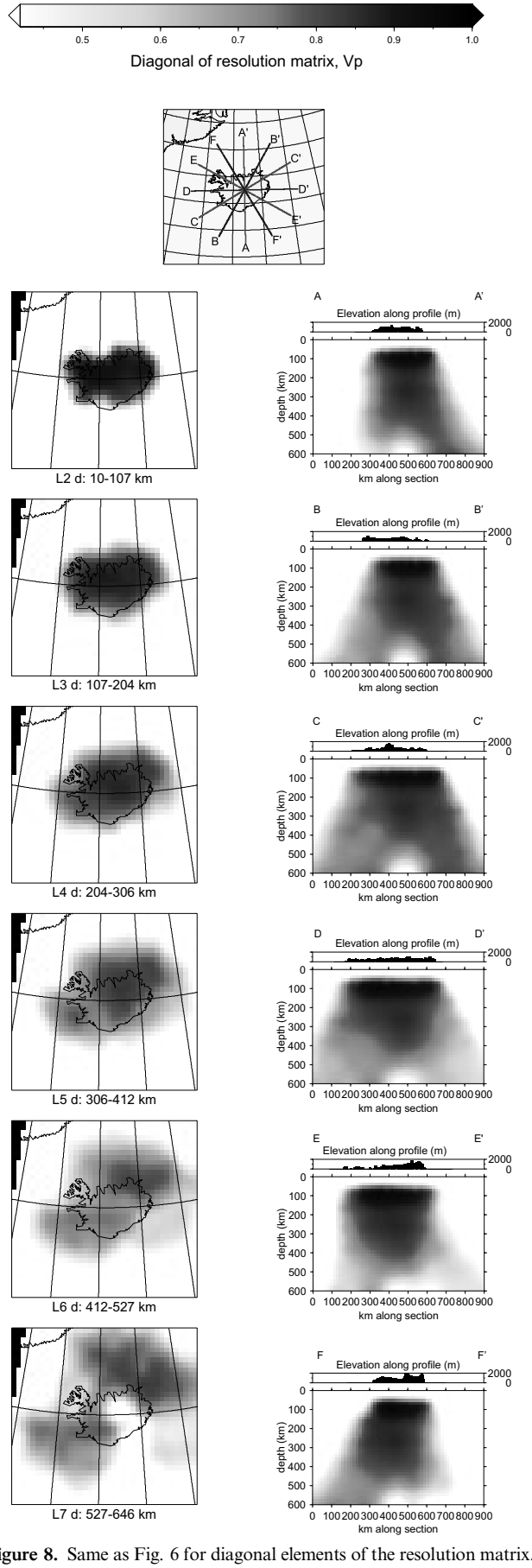

Figure 8. Same as Fig. 6 for diagonal elements of the resolution matrix.

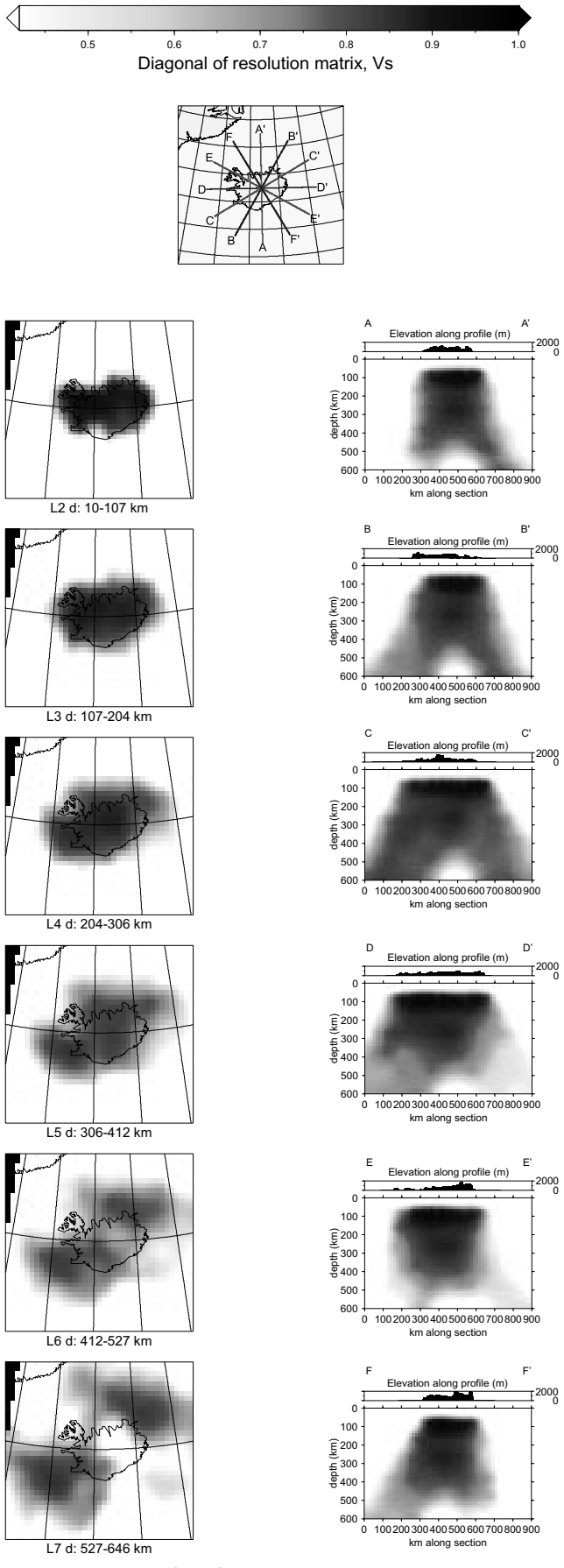

Figure 9. Same as Fig. 8 for V_S.

is always radial and outwards plunging. Because there are no outlying seismic stations at which to record waves traversing the study volume, deep, peripheral blocks on the edges are sampled only by rays approaching from outside the study volume. It is significant to our results that the radial smearing at the periphery is similar in all areas, and not greater in one quadrant than in another. Below ~450 km the tendency for downward smearing, and for structure outside the imaged volume to map into the model, is strong. Thus, despite the relatively high hit-counts and resolutions in some deeper areas, we consider our models to be unreliable at depths > ~450 km.

In order to increase our confidence in the large-scale first-order features of our models, we performed a fourth resolution test for both V_P and V_S. We generated models containing hypothetical wave-speed anomalies, expressed in the block structure used in our inversions, and multiplied the models by the computed resolution matrices **R** (eq. 1) for 100 km thick layers without offset-and-averaging. The results show how hypothetical anomalies would be distorted in the tomographic inversion because of uneven sampling by the available seismic rays. This test is more powerful than one based only on the diagonal elements of **R**, because it measures not only the sensitivity to an anomaly at a particular location, but also the tendency to generate spurious images in the wrong locations.

We tested whether we could faithfully image a simple, vertical, cylindrical, plume-like anomaly with constant wave speeds inside and outside. Fig. 12 shows the results of such a test for an anomaly with horizontal dimensions of 2×2 blocks (150 km × 150 km) underlying central Iceland. The result indicates that good resolution extends to depths of about 500 km in both V_P and V_S, and that there is little tendency to distort the shape of the anomaly in any systematic way. We performed tests of many such anomalies with different diameters and locations, all of which confirm this conclusion.

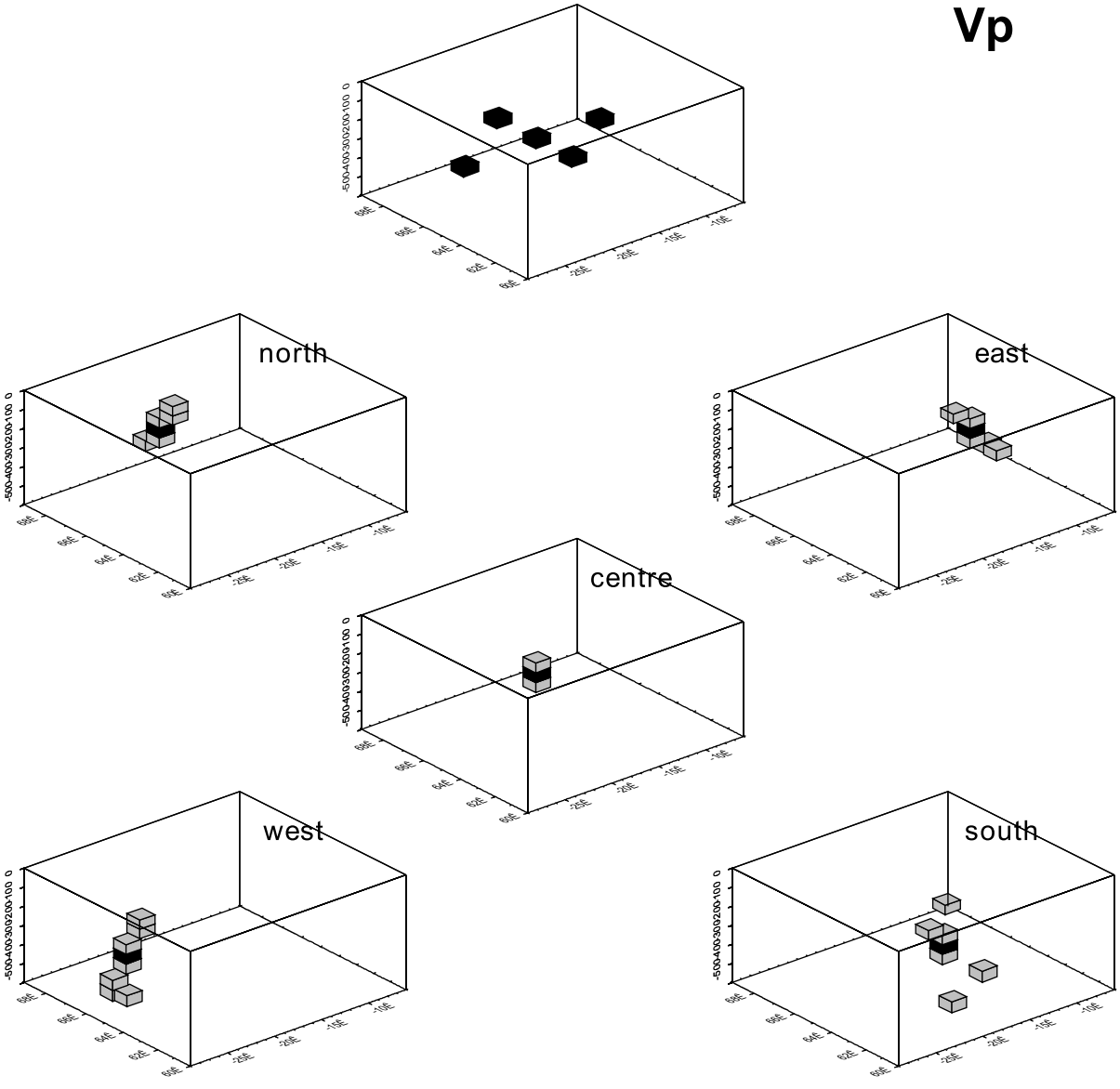

Figure 10. 'Volume metrics' for five blocks from the final V_P model (75 km wide blocks, 50 km thick layers), as seen looking downwards from the southwest. Top: locations of the five blocks, which lie in the layer at about 250–300 km depth. The five lower boxes show how anomalies located in the five black blocks are smeared (grey blocks) in the final model as a result of the ray distribution and the inversion method. The off-diagonal elements of the resolution matrix corresponding to the grey blocks sum to 0.95.

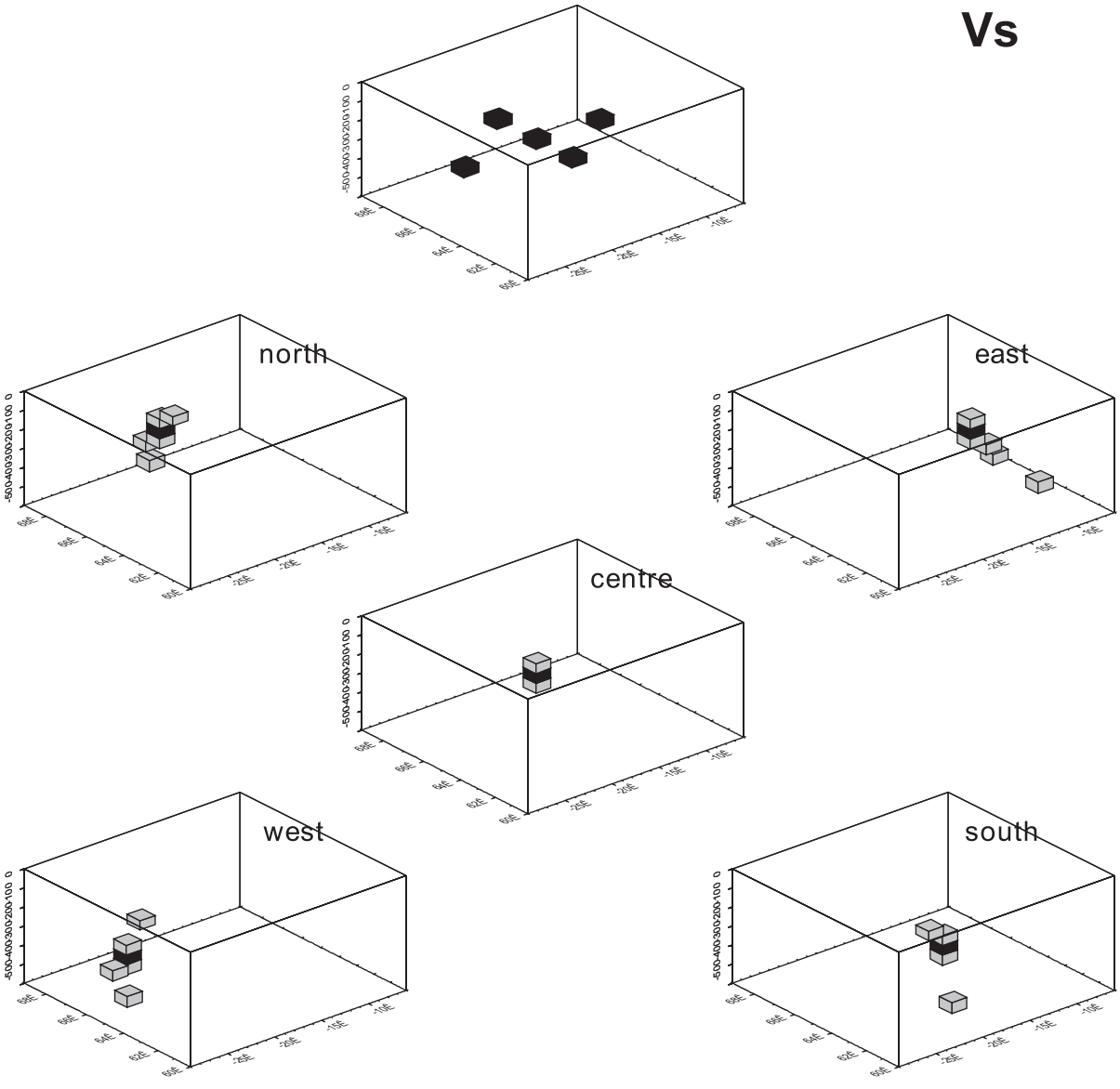

Figure 11. Same as Fig. 10 for V_S.

We also tested the ability of our method to resolve structure beneath the Tjörnes Fracture Zone to the north of Iceland. We found that such structure in the upper 100–300 km could be resolved clearly to a distance of ~50 km north of Iceland. There was no tendency for computed anomalies to be terminated artificially beneath the fracture zone.

RESULTS

Our final V_P model is shown in Fig. 13. The most significant feature is a coherent, low-V_P body extending vertically downwards beneath east-central Iceland. This anomaly has a strength of up to −2.7 per cent in the top layer (Fig. 13, layer L2), and up to −2.1 per cent in deeper layers.

Wave-speed variations in the special first layer are as strong as ±5.5 per cent for V_P and ±8 per cent for V_S, with little spatial coherence in their values (Fig. 13, layer L1). Recent explosion seismology, surface wave and receiver function work suggests that the crust is thickest (up to about 40 km) in central Iceland and thinner (around 25 km) beneath coastal areas (Darbyshire *et al.* 1998; Allen *et al.* 1999; Du & Foulger 1999, 2001; Du *et al.* 2001). The wave-speed perturbations in the special first layer show only very broadly such a trend, suggesting that they reflect mostly the very shallow structure of the upper 10 km only. Crustal structure below this contributes to the top layer of the tomographic image and to the strong V_P anomalies imaged there. It is a common problem in teleseismic tomography that few rays cross at shallow depths and shallow structure is thus poorly resolved. When an independently determined model for the seismic structure of the crust over all of Iceland becomes available, it will be possible to overcome this limitation by explicitly correcting for the crust in our model.

There are no crossing rays in the upper ~60 km of the model, which includes layer 2. In this layer, the structure determined is thus the smoothed perturbation field obtained independently for each station. The low-wave-speed anomaly is sharply truncated to the north, at the TFZ. It underlies the NVZ, EVZ and MVZ, and is centred easterly within the MVZ,

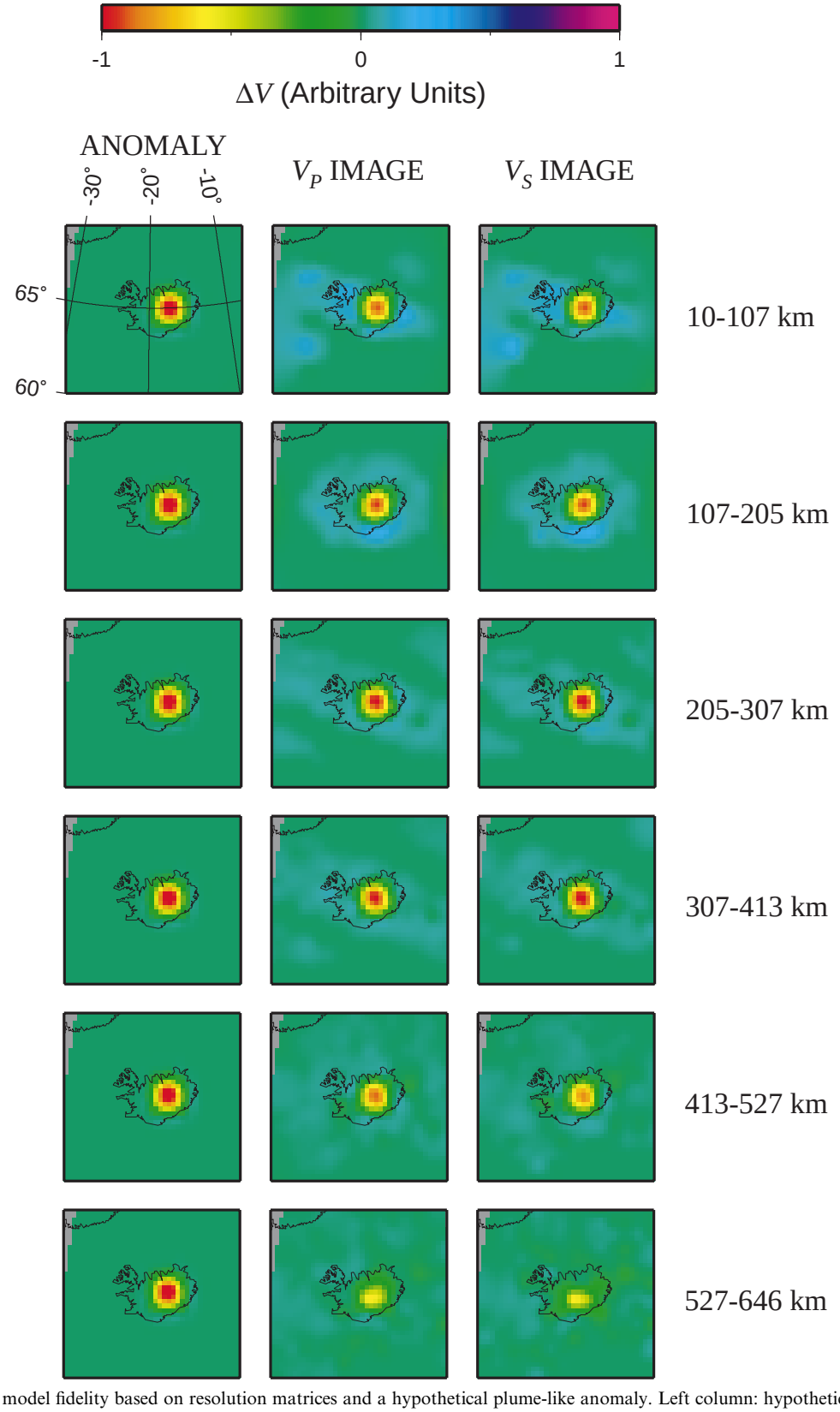

Figure 12. Test of model fidelity based on resolution matrices and a hypothetical plume-like anomaly. Left column: hypothetical vertical anomaly with horizontal dimensions of 2×2 blocks (150 km $\times$ 150 km). Middle column: result of multiplying the hypothetical model by the resolution matrix of the V_P model for 100 km thick layers. Right column: same as middle column for V_S. The structure is recovered well down to at least 500 km in both V_P and V_S, with strength reduced below 500 km and in the upper 200 km. There is no tendency to smear the anomaly preferentially in any direction. This test assesses the effect of non-uniform ray coverage and the performance of the inversion method, but does not quantify the effects of errors in the data, e.g. from picking, or approximations in the theoretical basis of the inversion technique.

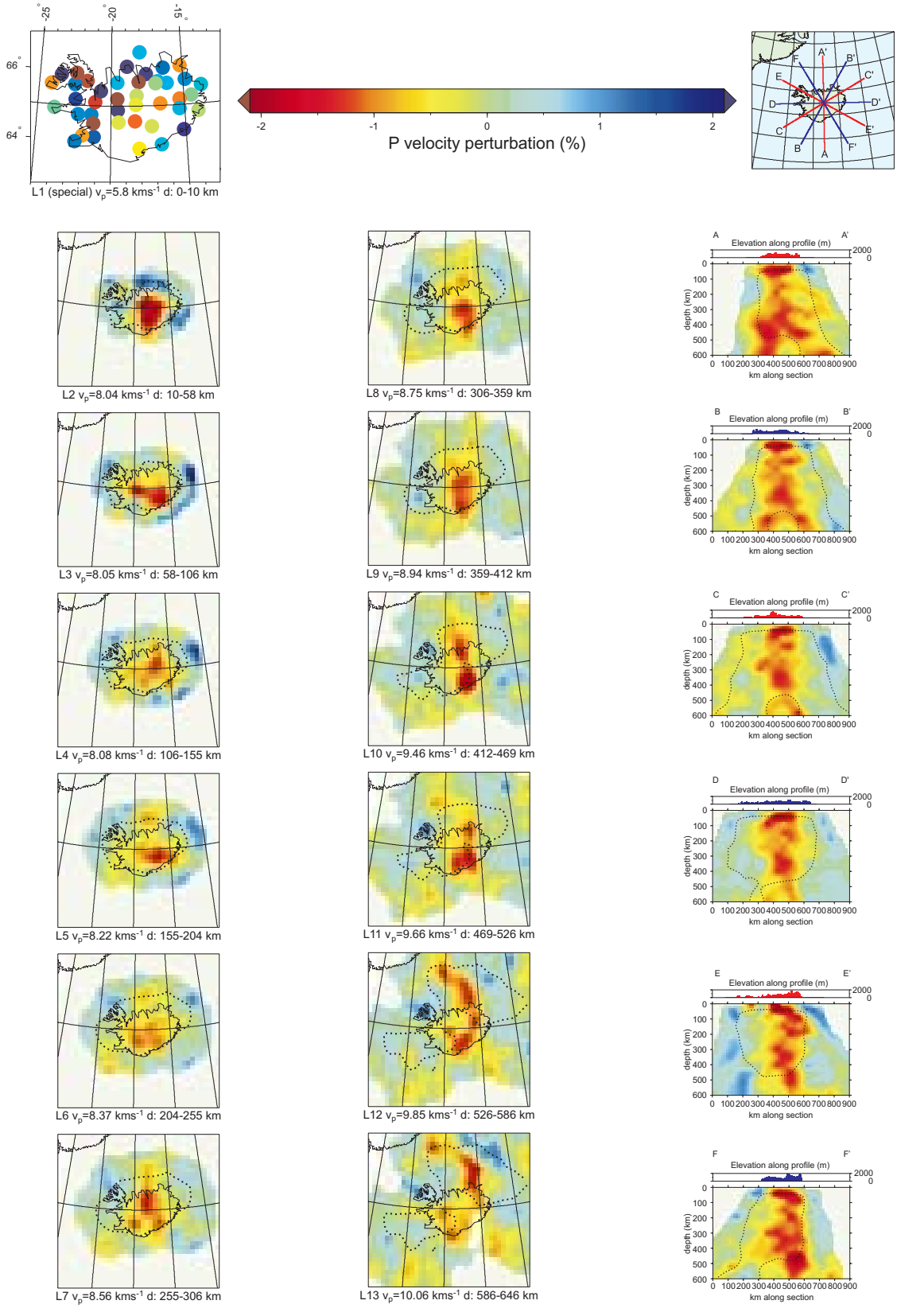

Figure 13. Horizontal (left and middle columns) and vertical (right column) sections through the final V_P model, which uses 75 km wide blocks and 50 km thick layers and was computed using the offset-and-averaging technique with $n=2$. The colour scale shows the percentage difference from V_P at the corresponding depth in the initial (IASP91) wave-speed model. The starting wave speed and the depth range are given beneath each horizontal section. Dotted black lines show the region within which resolution (the diagonal element of **R**) is ≥ 0.7. Maps are plotted in azimuthal-equidistant projection. Unmodelled areas are pale green or white. Top left: wave-speed perturbations in the 'special first layer'; top right: map showing lines of vertical sections.

between the glaciers Vatnajokull and Hofsjokull. A small, local, low-V_P anomaly occurs beneath the Northwest Fjords area. The area where V_P is depressed by more than 1 per cent relative to the surrounding areas has a diameter of 200–250 km.

In the depth interval ~50–250 km, the low-V_P anomaly underlies northwest Vatnajokull, the NVZ, EVZ and MVZ (Fig. 13, layers L3–L6). It extends beneath all of the MVZ at all depths, but is not everywhere continuous beneath the NVZ and EVZ. As a result, it is elongated east–west in some layers, most notably at depths of ~50–100 and ~150–200 km. A weak low-V_P anomaly underlies the Reykjanes ridge, southwest of Iceland, at all depths (Fig. 13, Section CC′). This part of our image is peripheral and the least reliable. The TFZ, in contrast, is well resolved in the upper ~450 km because of the presence of the station Grimsey off the north coast of the mainland (Fig. 1). The TFZ is underlain by relatively high-V_P material in the upper ~100 km (Fig. 13, section AA′), but beneath this V_P is low.

Beneath ~250 km, the morphology of the low-V_P anomaly changes systematically. Instead of being cylindrical, with a quasi-circular or east–west elongated shape in map view, it becomes elongated north–south. This is clear in all horizontal sections below this depth, down to the limit of moderate resolution at ~450 km (Fig. 13, layers L7–L10). This change from cylindrical to tabular morphology is particularly clear in cross-section. Section AA′ of Fig. 13 runs south–north and clearly shows the anomaly widening with depth, whereas the west–east section DD′ shows the anomaly narrowing with depth. The volume metrics show an equal tendency for the inversion to smear anomalies radially outwards and downwards in all directions, which suggests that this anomaly shape is not a result of smearing. Furthermore, images of hypothetical anomalies (Fig. 12) show no tendency to elongate real anomalies north–south. This supports our inference that the azimuthally asymmetric morphology we observe is real.

Because the maximum aperture of our array is ~450 km, structure imaged at depths greater than this is poorly resolved, and heavily influenced by downward smearing. This is a consequence of the inherent geometric weakness of teleseismic tomography, and stems from the fact that there are few crossing rays at great depth. Thus, despite the fact that the formal resolution is good in some parts of our model at greater depth, we do not attach significance to those parts of our model deeper than ~450 km, but show these results for information only. The low-wave-speed anomaly we image persists from the surface down to at least ~450 km depth, and thus our experiment does not image the base of the anomaly.

The structure obtained for V_S is shown in Fig. 14. Fewer *S*-wave than *P*-wave data were available, the picking accuracy was poorer because of the longer wavelength of *S* waves, and thus the image obtained is poorer than the V_P image. Most of the first-order features of the two models agree well, however. Again, the most obvious feature is a coherent, low-wave-speed body that extends throughout all well-resolved depths. The V_S anomaly has a strength of up to −4.9 per cent in the upper ~300 km and it extends beneath the MVZ, the NVZ and Vatnajokull (Fig. 14, layers L2–L7). A weak low-V_S anomaly underlies the Northwest Fjords in the top ~50 km. As with V_P, the V_S anomaly in the depth interval ~50–200 km is circular in map view or slightly elongated east–west. Low-V_S material underlies the Reykjanes ridge in the depth interval ~50–200 km, but not at greater depths (Fig. 14, Section CC′). In this area, the *S*-wave data set is larger than the *P*-wave data set and the model has better resolution. Beneath the TFZ, V_S is reliably resolved and is high in the upper ~100–150 km. The low-V_S anomaly beneath central Iceland extends beneath the TFZ only at depths greater than ~150 km. As for V_P, the V_S anomaly becomes tabular and oriented north–south at depth (Fig. 14, Sections AA′ and DD′).

Fig. 15 shows the distribution of the ratio V_P/V_S, represented as deviations from the IASP91 model (Fig. 16). The ratios shown are computed from the separate V_P and V_S models, obtained by adding the calculated anomalies to the IASP91 starting models. They are less well determined than either V_P or V_S because of the inhomogeneous sampling and resolution in the two models, because teleseismic tomography only determines wave-speed perturbations and is insensitive to absolute speeds, and because the errors in both wave-speed models contribute to the error in V_P/V_S (the relative variances add),

$$\frac{\mathrm{Var}(V_P/V_S)}{V_P^2/V_S^2} = \frac{\mathrm{Var}(V_P)}{V_P^2} + \frac{\mathrm{Var}(V_S)}{V_S^2}\,.$$

For this reason, V_P/V_S is moderately well resolved only on the scale of ~100 km and only down to the limit of good resolution, i.e. ~450 km depth.

The V_P/V_S anomaly is $\geq +1$ per cent beneath much of Iceland. It exceeds +3 per cent beneath the MVZ and northwest Vatnajokull in the depth range ~100–200 km and beneath the MVZ, EVZ and NVZ in the depth range 200–300 km. V_P/V_S is also exceptionally high at depths of 100–200 km beneath the Reykjanes ridge, where the anomaly exceeds +2 per cent, but it is normal beneath the TFZ in the upper ~100 km, and only slightly high at greater depth. In the depth range ~300–400 km, V_P/V_S anomalies greater than +2 per cent are found only in peripheral, less reliable parts of the model.

In addition to the first-order features described above, our V_P, V_S and V_P/V_S models shown in Figs 13, 14 and 15 display small-scale, second-order features that have not been suppressed by heavy smoothing in the inversion method as is the case in some studies (e.g. Wolfe *et al*. 1997). The consistency of these features varies between inversions with different block sizes, damping, layer thicknesses and input data. These features are probably not all significant and may be due to data noise or to real structure, and we do not consider them sufficiently reliable to warrant detailed interpretation. Smoother and rougher inversion results obtained with different damping and parametrizations are given by Pritchard (2000).

INTERPRETATION AND DISCUSSION

The main anomaly

The first-order observation is of a vertically extensive, low-wave-speed body centred beneath the middle of Iceland. In the upper ~50 km, the body is centred easterly beneath the MVZ, not beneath northwest Vatnajokull, where the hotspot centre is traditionally assumed to lie. Our result agrees with gravity data and crustal structure. The centre of the Bouguer gravity low over Iceland lies in the eastern MVZ (Thorbergsson *et al*. 1990), where seismic receiver-function data show a thick, low-velocity zone in the lower crust (Du & Foulger 2001; Du *et al*. 2001). Low wave speeds are present at all depths beneath the MVZ, and a positive V_P/V_S anomaly, which suggests the presence of

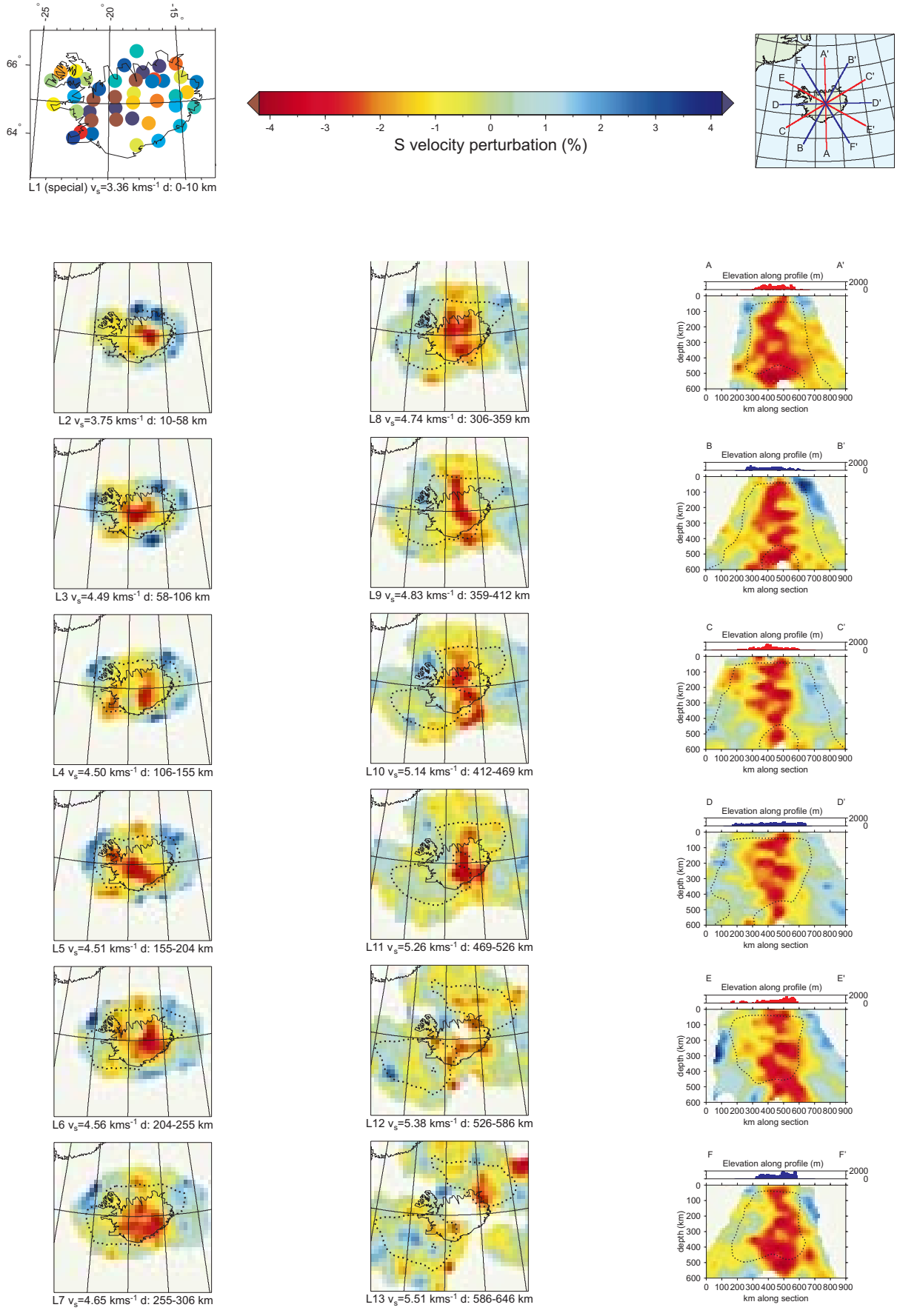

Figure 14. Same as Fig. 13 for V_S.

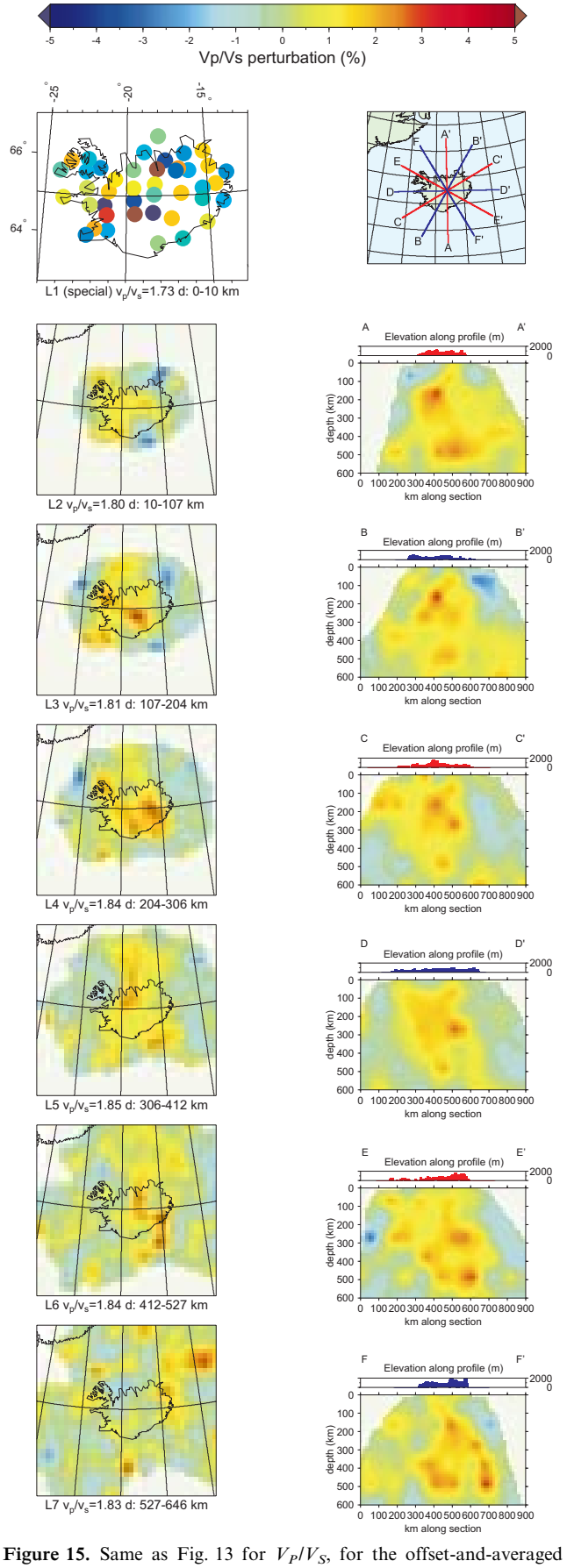

Figure 15. Same as Fig. 13 for V_P/V_S, for the offset-and-averaged model with 75 km wide blocks and layers 100 km thick.

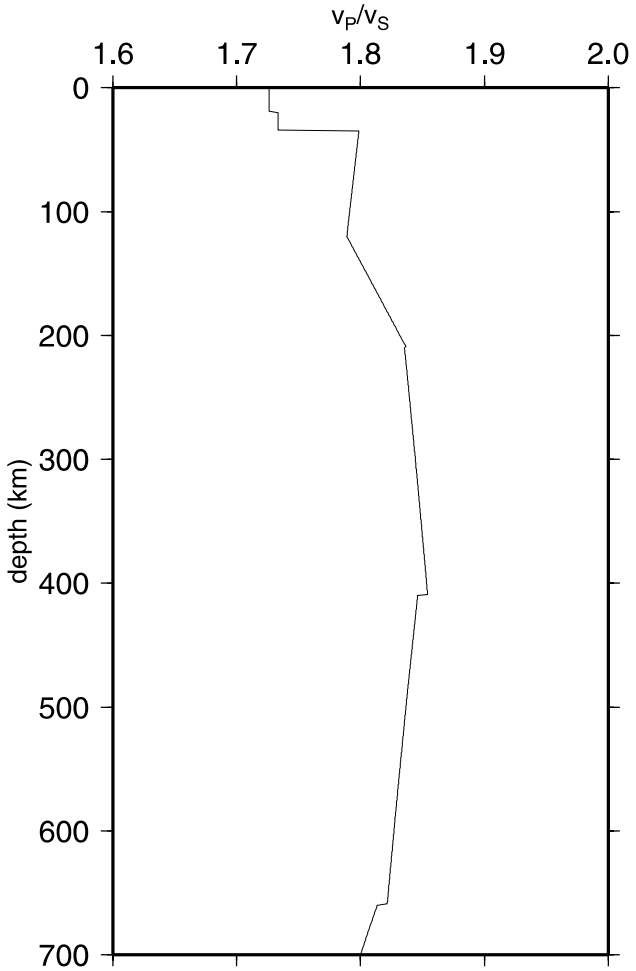

Figure 16. Variation of V_P/V_S with depth in the IASP91 model, i.e. the starting values of V_P/V_S (Kennett & Engdahl 1991).

partial melt, occupies the depth range ~100–200 km. In contrast, the anomaly is discontinuous beneath the NVZ and EVZ, suggesting that these linear zones may be fed laterally by a central upwelling. The WVZ is peripheral to the main, low-wave-speed body at most depths, in keeping with the view that it is a declining rift (Sigmundsson *et al.* 1994). A subsidiary, 15 mGal Bouguer gravity low is associated with the Northwest Fjords area, where we image local low V_P and V_S anomalies in the upper ~50 km.

A number of factors affect seismic wave speeds. High temperature reduces V_P by ~0.9 per cent per 100 K and V_S by 1.2–1.8 times this (Anderson 1989; Faul *et al.* 1994; Ito *et al.* 1996; Goes *et al.* 2000). Numerical plume models for Iceland predict temperature anomalies of 70 to 250 K (e.g. Sleep 1990; Feighner & Kellogg 1995; Ribe *et al.* 1995; White *et al.* 1995), which correspond to anomalies in V_P of 0.6–2.2 per cent and in V_P/V_S of up to 2.1 per cent. The anomalies we observe are locally up to about −2 per cent in V_P and +3.7 per cent in V_P/V_S, although the bulk of the low-wave-speed body has an anomaly in V_P of 0.5–1.5 per cent and in V_P/V_S of ~1 per cent (Figs 13 and 15).

The wave-speed anomalies cannot be caused solely by elevated temperatures, since V_S anomalies of up to 4.9 per cent would imply temperature anomalies of up to ~300 K, thought to be an unrealistically high value. Furthermore, V_P/V_S

anomalies of only up to ~2.5 per cent would be expected. Partial melt is a candidate explanation for the observations, as it depresses V_S more strongly than V_P (Anderson 1989; Karato 1993). The effect of melt on seismic wave speeds is difficult to assess quantitatively, because it depends strongly on the geometry of the melt bodies, with tabular shapes such as dykes, sills and thin films having about twice the effect of tubular shapes (Spetzler & Anderson 1968; Anderson & Sammis 1970; Faul *et al.* 1994). Melt may form at grain boundaries as both films and pockets (Faul *et al.* 1994). Under these circumstances, a decrease of ~3.4 per cent in V_P and 7.8 per cent in V_S for each 1 per cent increase in melt is a reasonable estimate (Goes *et al.* 2000). In the upper ~300 km of the central core of the body, where the V_P/V_S anomaly is strong, the observations are most readily explained by temperature anomalies significantly lower than 200 K and a few tenths of a per cent partial melt. Such an amount is insufficient for percolation to take place (Faul *et al.* 1994; Schmeling 2000). The outer parts of the body can be explained by lower temperature anomalies and per cent partial melt. Regions where V_P/V_S is highest and V_P lowest are the most likely sites for partial melt. These underlie the MVZ and northwest Vatnajokull in the depth range ~100–200 km, and the NVZ and EVZ in the depth range ~200–300 km.

The degree of partial melting suggested by our observations is smaller, and the depth range greater, than predicted for spreading plate boundaries and plumes. Melt fractions up to ~20 per cent are predicted to occupy zones a few tens of kilometres high in the upper ~70 km beneath ridges and ~120 km of plumes (Iwamori *et al.* 1995; Shen & Forsyth 1995; White & McKenzie 1995; Ito *et al.* 1996; Schmeling 2000). Such zones are too small to be resolved by teleseismic tomography, which will, at best, average them over a large volume. However, the distribution of low-concentration partial melt beneath hotspots and ridges is not strongly constrained by physical plume models (McKenzie & Bickle 1988). Our observations are consistent with Iceland being underlain by an extensive volume of low-degree partial melt that extends at least throughout the sub-lithospheric low-velocity zone in the depth interval 190–250 km (Gutenberg 1959; Anderson & Bass 1984; Anderson 1989).

Other factors expected to affect seismic wave speeds in a volcanic environment are chemical heterogeneity, including chemical depletion, and anisotropy. The possibility that compositional variation might contribute to the observed anomalies cannot be ruled out. Depletion is the removal of basalt from the parent rock. V_P increases by ~0.5 per cent per 10 per cent depletion (Goes *et al.* 2000), and partial melting levels of up to ~20 per cent are predicted locally beneath Iceland (White & McKenzie 1995). However, the parent volume must be continuously replenished by flow from deeper levels if erupted lavas are not to become progressively depleted with time, and if melt production is not eventually to dwindle and cease, trends that are not observed. The degree of depletion beneath Iceland is thus not certain, nor is its expected effect on seismic wave speeds.

Anisotropy is expected at mid-ocean ridges because flow aligns olivine crystals so that the crystallographic *a*-axes [100] lie parallel to the flow direction. This causes V_P and V_S to be higher for waves propagating parallel to the direction of flow than normal to it. Such anisotropy might be as strong as +7 per cent (e.g. Anderson 1989; Kendall 1994). A simplistic model for a plume beneath Iceland would predict vertical upward flow within a central core and radially outward flow in the upper 50–100 km. Superimposed on the shallow, radial flow pattern might be bilaterally symmetric flow away from the spreading plate boundary. Such a pattern of flow might increase vertical wave speeds in the plume core, where rays are subvertical. Thus the negative wave-speed anomalies we observe there, of up to −2.1 per cent in V_P and −4.9 per cent in V_S, if corrected for anisotropy, might be as strong as −9 and −12 per cent. In the topmost ~100 km, dykes and flow-induced anisotropy might strengthen the negative anomalies observed, since horizontal flow aligns the slow *b*-axis vertically. However, the few observations of upper mantle anisotropy currently available for Iceland fail to support the simple flow model described above (Bjarnason *et al.* 1996), so this effect cannot yet be assessed quantitatively.

Structure beneath the Reykjanes ridge and the Tjornes Fracture Zone

We observe a negative V_P anomaly of up to ~−0.5 per cent at all depths beneath the Reykjanes ridge close to Iceland. Resolution in V_S is superior in this part of the model, and shows an anomaly of up to ~−2.5 per cent in the depth range ~50–200 km. In this region, the V_P/V_S anomaly is up to +2.4 per cent, which is consistent with the presence of up to a few tenths of a per cent of partial melt. The Reykjanes ridge is peripheral to our study volume and is poorly imaged. However, the structure imaged beneath it contrasts with that observed beneath other seaward parts of our study volume, for example, to the west and east of Iceland (Figs 13 and 14, section DD′). This structure is also expected on geological grounds, and is thus probably real.

The structure found beneath the TFZ to the north is well resolved and contrasts sharply with that beneath the Reykjanes ridge. Both V_P and V_S are normal or high in the upper 100–200 km. At greater depths, the low-wave-speed body imaged beneath central Iceland extends to the north of the TFZ. The positive V_P/V_S anomaly is, however, no stronger than ~+1 per cent anywhere beneath this region, and thus partial melting is not required to explain the observations.

The structures we observe beneath the Reykjanes ridge and the TFZ agree with predictions that melt may be channelled beneath ridges and blocked by fracture zones (e.g. Vogt 1976; Schilling *et al.* 1985; Schilling 1991; Ribe *et al.* 1995; Sleep 1996, 1997). Material is thought to flow unimpeded from beneath central Iceland southwestwards along the Reykjanes ridge at shallow depth, and to cause the topographic uplift and enhanced on-ridge volcanism observed there. The structure we observe beneath the TFZ supports the prediction that this fracture zone blocks the lateral flow of melt. This close agreement with geological ground truth in peripheral parts of our study volume strengthens confidence in our results in general.

Nature of the anomaly beneath Iceland

The most significant feature of the anomaly is its change in shape from cylindrical to tabular at about 250 km depth beneath Iceland. Several geodynamic models predict such a change in morphology, including buoyant upwelling, passive infilling of a widening rift, convection resulting from lateral temperature gradients, heating from below or cooling from above. All these models imply that the anomaly is caused by a buoyant upwelling whose origin is approached at the depth

at which it becomes tabular. Thus, although our experiment does not resolve structure below the base of the anomaly, the change in morphology we observe suggests that the anomaly is confined to the upper mantle. We cannot rule out by direct observation the possibility that it continues below this, but some unknown mechanism would be required to cause a cylindrical plume rising from deep within the lower mantle to become tabular as it rises. The possibility that the tabular structure is an artefact of poor resolution and that the true structure is axisymmetric is shown to be very unlikely by the several resolution tests we performed (see e.g. Figs 10 and 12).

Numerical models of convection in a constant-viscosity layer heated both from below and internally display changes in thermal structure resembling the structure we observe (Houseman 1990). Both uprising hot bodies and downgoing cold bodies are predicted to start out with tabular morphology and then to become cylindrical. Flow at the surface retains memory of the deep upwellings, so that surface rift zone orientations reflect the trends of the deep tabular zones near the base of the convecting layer. Although convection modelling results are not unique, they do predict a morphological change such as that we observe, in addition to the fact that the tabular part of the anomaly below 250 km underlies the spreading plate boundary and has the same orientation.

Pulling apart lithospheric plates induces transient upwelling on a vertical scale similar to lithospheric thickness (Anderson 1998a), which in the case of the Greenland and Scandinavian cratons is $\sim$200–300 km. The deep upwelling is predicted to have a linear form parallel to the plate margins at depth, but to assume a more cylindrical shape at shallower levels (Korenaga 2000). Lateral temperature gradients at the edges of cold cratons can also drive convection (e.g. King & Anderson 1995, 1998; Anderson 1998a). Sinking cold mantle material at the margins of Greenland and Scandinavia might by this mechanism induce compensating upwelling of hot material centred between the cratons, and could account for volcanism in the Iceland region. 3-D models of this process indicate that a north–south tabular upwelling is expected at depth, which becomes concentrated upwards into cylindrical bodies (Korenaga 2000).

Morphological changes like the one we observe are common in other geological phenomena, e.g. salt domes, diapirs and back-arc volcanism. Similar structures also occur in laboratory experiments on diapiric phenomena in materials such as oils and putty, and in gravity-driven and centrifuged models (Ramberg 1981). Our model is probably the first observation of such morphology on the scale of the upper mantle.

All the above-mentioned models predict that the Iceland hotspot has remained essentially centred in the middle of the north Atlantic for its whole history. Such a conclusion would support ridge-stationary models (e.g. Bott 1985) but not models of an eastward-migrating hotspot (e.g. Vink 1984), which are based on the assumption that the Iceland hotspot has remained fixed relative to other Atlantic hotspots.

Comparison with whole-mantle and regional full-thickness mantle tomography models

Our inference that upwelling beneath Iceland is primarily an upper mantle phenomenon is consistent with recent whole-mantle and regional full-thickness mantle tomography models, which provide no evidence for structure in the lower mantle comparable to that in the upper mantle. Following the pioneering studies of Hager & Clayton (1989) and Zhou (1996), studies by Bijwaard & Spakman (1999), Ritsema *et al.* (1999), Megnin & Romanowicz (2000) and Karason & van der Hilst (2001a,b) all confirm that a strong, negative wave-speed anomaly 1000 km or more wide occupies the upper mantle beneath the Iceland region. Because of the resolution limitations in these studies, the results are consistent with the narrower but stronger anomaly we observe, and all the results are consistent with a narrow anomaly embedded in a broader, weaker anomaly extending beyond our study volume. All these studies image a strong anomaly that is confined to the upper mantle. Anomalies in the lower mantle are weak, with strengths of at most a fraction of a per cent, have complicated shapes and are mostly discontinuous with the upper mantle anomaly immediately beneath Iceland. Resolution may not be equally good at all depths, however, and it is important to explore, for each study, the minimum size and strength of anomaly in the lower mantle that can be ruled out.

Ritsema *et al.* (1999) inverted more than two million data from digital global and regional networks, including shear wave arrival times (*S*, *SS*, *SSS*, *ScS* and *SKS*), fundamental- and higher-mode Rayleigh wave phase velocities and normal-mode frequencies. This is the first whole-mantle tomography model that makes use of higher-mode phase velocity measurements. The inclusion of higher-mode surface waves results in this model probably having the best resolution of any spherical harmonic model to date in the transition zone and mid-mantle. Resolution beneath Iceland and the north Atlantic is further improved by the use of *SS* and *SSS* traveltimes from stations in North America and Europe, for which the bounce points underlie Iceland and the north Atlantic (J. Ritsema, personal communication, 2001). In this model, lower mantle V_S anomalies beneath Iceland are clearly much weaker and less coherent than the upper mantle anomaly, and there is no evidence that the latter continues down into the lower mantle (Fig. 17).

Megnin & Romanowicz (2000) inverted time-domain waveforms of S_H body waves and first- and second-orbit fundamental- and higher-mode Love waves, which have sensitivity throughout the mantle. Their method uses more accurate kernels for body waves in the lower mantle than traveltime methods that assume infinite-frequency or waveform methods that use path-averaging approximations (Megnin & Romanowicz 1998). Their V_S model resembles that of Ritsema *et al.* (1999) in having weak lower mantle anomalies beneath Iceland (Fig. 18). In the upper few hundred kilometres of the lower mantle, their model has a positive V_S anomaly.

Bijwaard & Spakman (1999) inverted a large set of reprocessed seismological bulletin *P*-wave arrival times (Engdahl *et al.* 1998). Their 3-D model has a continuous, negative V_P anomaly in the lower mantle with a strength of up to -0.5 per cent, extending from a few hundred kilometres above the core–mantle boundary beneath the Iceland–Greenland ridge to the base of the upper mantle transition zone beneath the Iceland–Faeroe ridge (Fig. 19a). The width of the anomaly varies from less than 300 to about 900 km, and it is inclined by about 30° from the vertical. Bijwaard & Spakman (1999) suggested that this anomaly represents a plume extending from the core–mantle boundary to the surface, and present a cross-section showing a continuous low-wave-speed structure throughout the upper and lower mantles (Fig. 19a). However, the impression of a continuous, homogenous structure is achieved by saturating

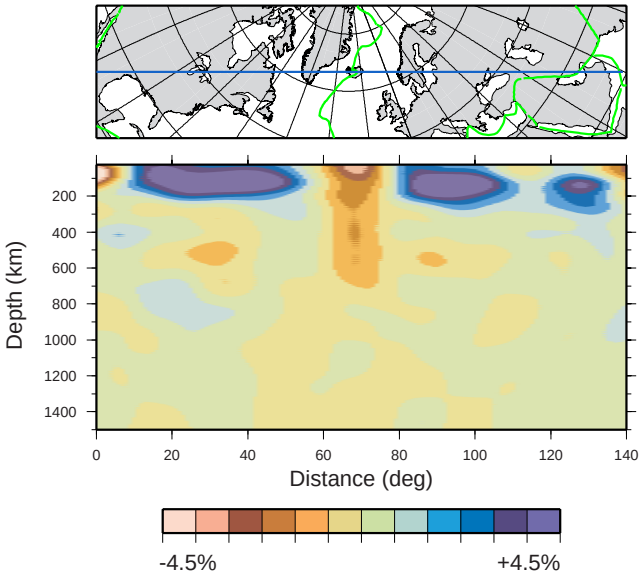

Figure 17. Cross-section at Iceland through the whole-mantle tomography model of Ritsema *et al.* (1999) (courtesy of J. Ritsema).

the colour scale at 0.5 per cent, concealing the fact that the anomaly is an order of magnitude stronger in the upper mantle than in the lower mantle. Furthermore, the limited longitudinal extent of the cross-section presented conceals the fact that similar, vertically continuous, even more plume-like, low-wave-speed structures are also imaged beneath the adjacent Canadian and Scandinavian cratons, where there is no geological evidence for hotspots. These facts, combined with the poor repeatability of this structure between independent models, makes it unlikely that the structure imaged represents a continuous plume traversing the whole mantle beneath Iceland. Furthermore, inversions heavily reliant on reprocessed seismological bulletin *P*-wave arrival times have very little resolving power in the lower mantle beneath Iceland (Karason & van der Hilst 2001a,b).

This last point is well illustrated in a study by Karason & van der Hilst (2001a,b) who used ∼seven million reprocessed *P*-, *pP*- and *PKP*-phase arrival times from the catalogue of Engdahl *et al.* (1998) measured at ∼4000 stations worldwide, from ∼300 000 earthquakes, along with several thousand differential traveltimes of *Pdiff*, *PKP* and *PP* waves determined by waveform cross-correlation. This data set was inverted for

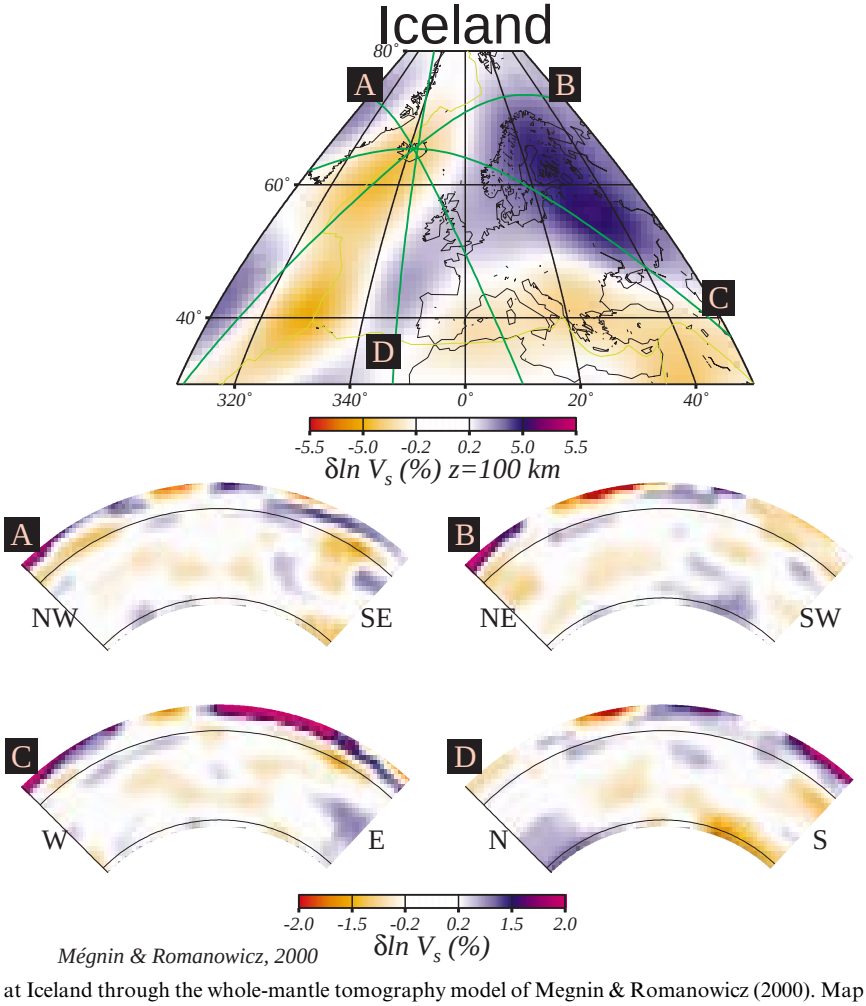

Figure 18. Cross-sections at Iceland through the whole-mantle tomography model of Megnin & Romanowicz (2000). Map at top shows anomalies at 100 km depth (courtesy of C. Megnin and B. Romanowicz).

global mantle structure using 3-D sensitivity kernels and local basis functions of variable size (Fig. 19b). Beneath Iceland, a low-wave-speed anomaly of up to 2 per cent is detected that extends from the surface down to the base of the upper mantle and no deeper (Fig. 19b, cross-section at lower left). In order to study the variation in resolution in the mantle beneath Iceland, and specifically to investigate if a deeper structure could be detected if it existed, rays were traced through a theoretical plume-like structure (Fig. 19b, cross-section at lower middle) to generate synthetic data. The theoretical structure extends from the surface to 1500 km depth, and has a wave-speed anomaly of 2 per cent in the upper mantle and 1 per cent in the lower mantle. The synthetic data were inverted to test for anomaly retrieval (Fig. 19b, cross-section at lower right). Retrieval of the anomaly is good above ~400 km, partial in the transition zone, but poor in the lower mantle. Inversion parameters can perhaps be found that would recover better this particular theoretical structure, but this example (H. Karason & R. D. van der Hilst, personal communication, 2001) illustrates that, with this data set, and that of Bijwaard & Spakman (1999) because of the paucity of rays sampling the lower mantle beneath Iceland, resolution there is very poor. This analysis illustrates the non-uniformity of data coverage, and thus resolution, in mantle tomography images, and the importance of assessing resolution prior to interpreting the results.

Presently available tomography models using spherical harmonic basis functions cannot resolve the sizes of bodies smaller than ~1000 km in diameter. Smaller bodies can be detected if they are strong, but they become smeared over broad regions. For example, low-wave-speed bodies underlying the mid-Atlantic ridge are imaged, but smeared over distances of ~1000 km, although regional and local-scale studies show them to be much narrower. Models that use local rather than spherical harmonic basis functions can resolve the sizes of smaller bodies. In addition, low-wave-speed bodies are more difficult to detect using tomography than high-wave-speed bodies because rays passing through a low-wave-speed body may not arrive first at stations. Beneath Iceland, ray coverage in the lower mantle is sparse for direct *P* waves, compared with the upper mantle, and the use of additional phases and higher-mode surface waves is necessary to achieve good resolution in the transition zone and uppermost lower mantle. Mindful of these caveats, it remains the case that none of the presently available tomographic models of the whole mantle shows evidence of continuation into the lower mantle of the structure imaged in the upper mantle beneath Iceland.

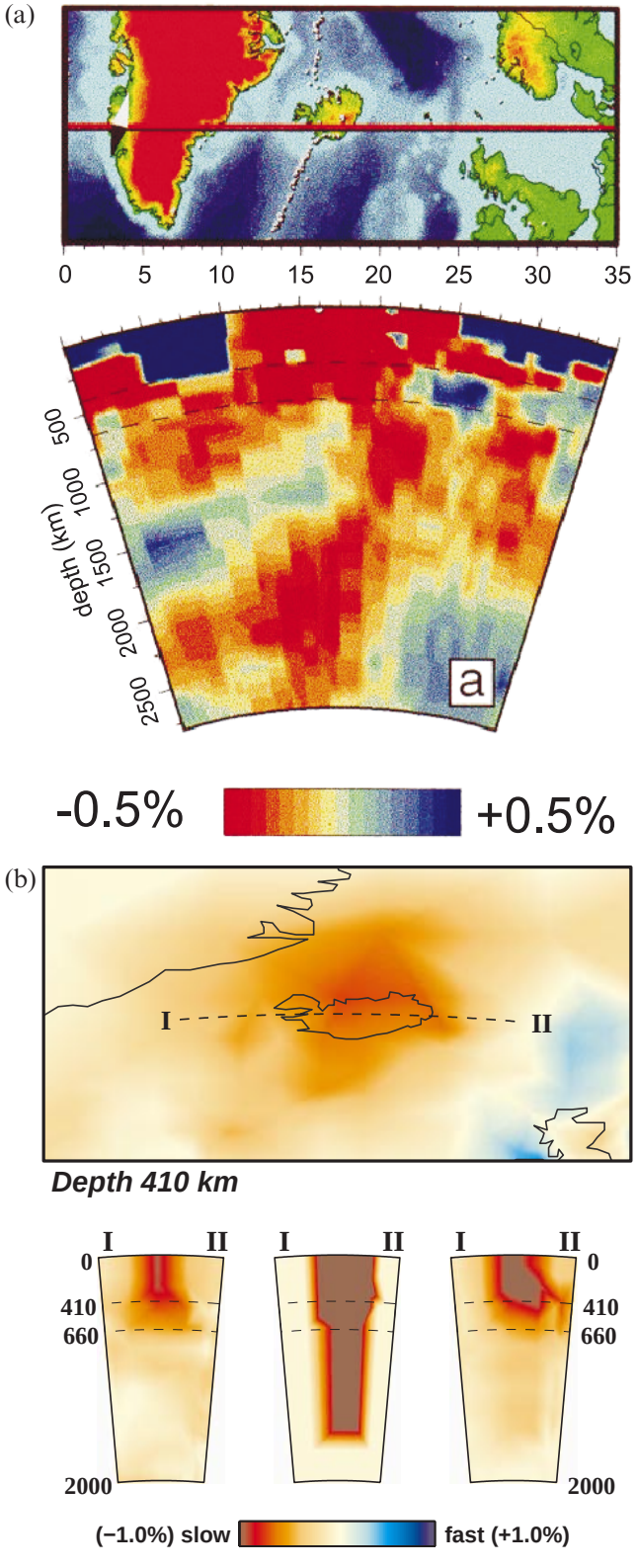

Figure 19. (a) Cross section through the Iceland region showing the full-thickness mantle *P*-wave tomographic model of Bijwaard & Spakman (1999). Upper panel shows line of cross section and lower panel shows cross section through the mantle. The impression of a uniform structure that is continuous from the surface to the core-mantle boundary is achieved by saturating the colour scale at ~10% of the maximum anomaly in the upper mantle. The limited lateral extent of the cross section conceals the fact that anomalies of a similar strength in the lower mantle underlie the adjacent Scandinavian and Canadian cratons (adapted from Bijwaard & Spakman, 1999). (b) Cross-sections at Iceland through the full-thickness mantle tomography model of Karason & van der Hilst (2001a,b). Map at top shows anomalies at 410 km depth. Row of cross-sections shows (left) inversion results and (middle) model of a theoretical plume-like anomaly extending from the surface to 1500 km depth, with wave speed 2 per cent low in the upper mantle and 1 per cent low in the lower mantle. Rays were traced through this model. Right: model retrieved from inversion of rays traced through the theoretical model shown in the middle cross-section. The same inversion parameters were used as for the model shown in the left cross-section (figure courtesy of Hrafnkell Karason).

The dependence of seismic wave speeds on temperature is weaker in the lower than in the upper mantle, so that a given temperature anomaly would be characterized by a weaker seismic anomaly in the lower mantle than in the upper mantle. However, the effect of temperature on seismic wave speeds is closely related to thermal expansion through the second Gruneisen parameter, both being caused by anharmonicity of lattice vibrations (e.g. Anderson 1989, Chapter 5), so material with a weak seismic anomaly in the lower mantle would have weak buoyancy. This fact suggests that material in the upper and lower mantles with greatly contrasting seismic anomalies would not form a single, coherent, convecting structure.

Comparison with previous teleseismic tomography results

Tryggvason *et al*. (1983) conducted the first teleseismic tomography study of the upper mantle beneath Iceland. They used data from a highly non-uniform 39-station network of 4 Hz geophones with pen-and-ink recording (Fig. 20). These data are of poor quality, because the geophones used are insensitive to teleseismic *P* waves, whose dominant frequencies are in the band $\sim$0.5–2.0 Hz. A set of 714 *P*-phase arrival times from 61 earthquakes was inverted to determine the V_P structure of the upper 375 km (Table 2). The resulting model has two disconnected bodies about 200 km in diameter with V_P up to ~ -3 per cent low (Fig. 21). This study did not deal with the effects of lateral variation in crustal structure, and explained only 33 per cent of the arrival time residual variance, which suggests that the data set contains little coherent signal. There is little resemblance between the results of Tryggvason *et al*. (1983) and those of later work.

Wolfe *et al*. (1997) conducted a study using data from a 16-station network of digital broad-band stations, uniformly distributed at intervals of $\sim$100 km over a 450 km $\times$ 260 km area covering much of Iceland (Fig. 22). They inverted 601 *P*-wave (mostly *P*-phase) times from 86 earthquakes and 560 *S*-wave (mostly *S*-phase) times from 78 earthquakes for structure in the upper 400 km, using station terms to model the crust. They achieved arrival time residual variance reductions of 90 per cent for *P* and 83 per cent for *S* (Table 2). They used a fine-scale (25 km) parametrization of the structure and applied smoothing constraints using a minimum-variation method to stabilize the inversion. The first-order structure they found is a negative wave-speed anomaly with a maximum strength of about -2 per cent for V_P and -4 per cent for V_S. In the shallowest parts of the model (125 km), this anomaly underlies the surface rift zones, and it broadens with depth to a width of $\sim$400 km at 400 km depth.

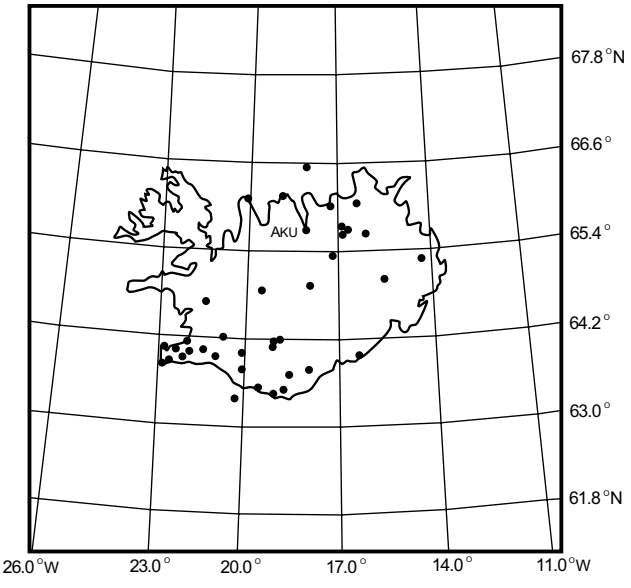

Figure 20. The permanent 39-station network of 4 Hz geophones used in the teleseismic tomography study of Tryggvason *et al*. (1983).

Compared with the experiment of Wolfe *et al*. (1997), our network contained about three times as many stations and had a larger aperture, including instruments in the far north and east of Iceland, on the island of Grimsey in the TFZ and on the tip of the Snaefellsnes peninsula. Our *P*-wave data set is more than five times as large and our *S*-wave data set over twice as large. In addition, we used many surface-reflected (*PP*, *SS*) arrivals, which improved ray coverage in azimuth–slowness space and model resolution. Wolfe *et al*. (1997) used an iterative method to deal with non-linearity effects of the refraction of rays, and smoothed their model by applying regularization constraints that minimize spatial gradients and roughness and minimize shallow or abrupt anomalies. Their model is thus highly smoothed, as it must be for such a sparse network.

Table 2. Details of teleseismic tomography studies of the upper mantle beneath Iceland.

	Tryggvason *et al*. (1983)	Wolfe *et al*. (1997)	This study
No. stations	39	16	42
Sensor type	4- Hz geophones	broad-band	broad-band
Block sizes horiz./vert. (km)	$\sim$150/75 & 100	25/25 00	75/50
Station terms?	no	yes	yes
No. earthquakes	61	86	113
No. *P* phases	61		160
No. P obs	**714**	**601**	**3159**
No. earthquakes	–	78	66
No. *S* phases	–		73
No. *S* obs	**–**	**560**	**1338**
Variance reduction *P*/*S*	33%	90%/83%	84%/89%

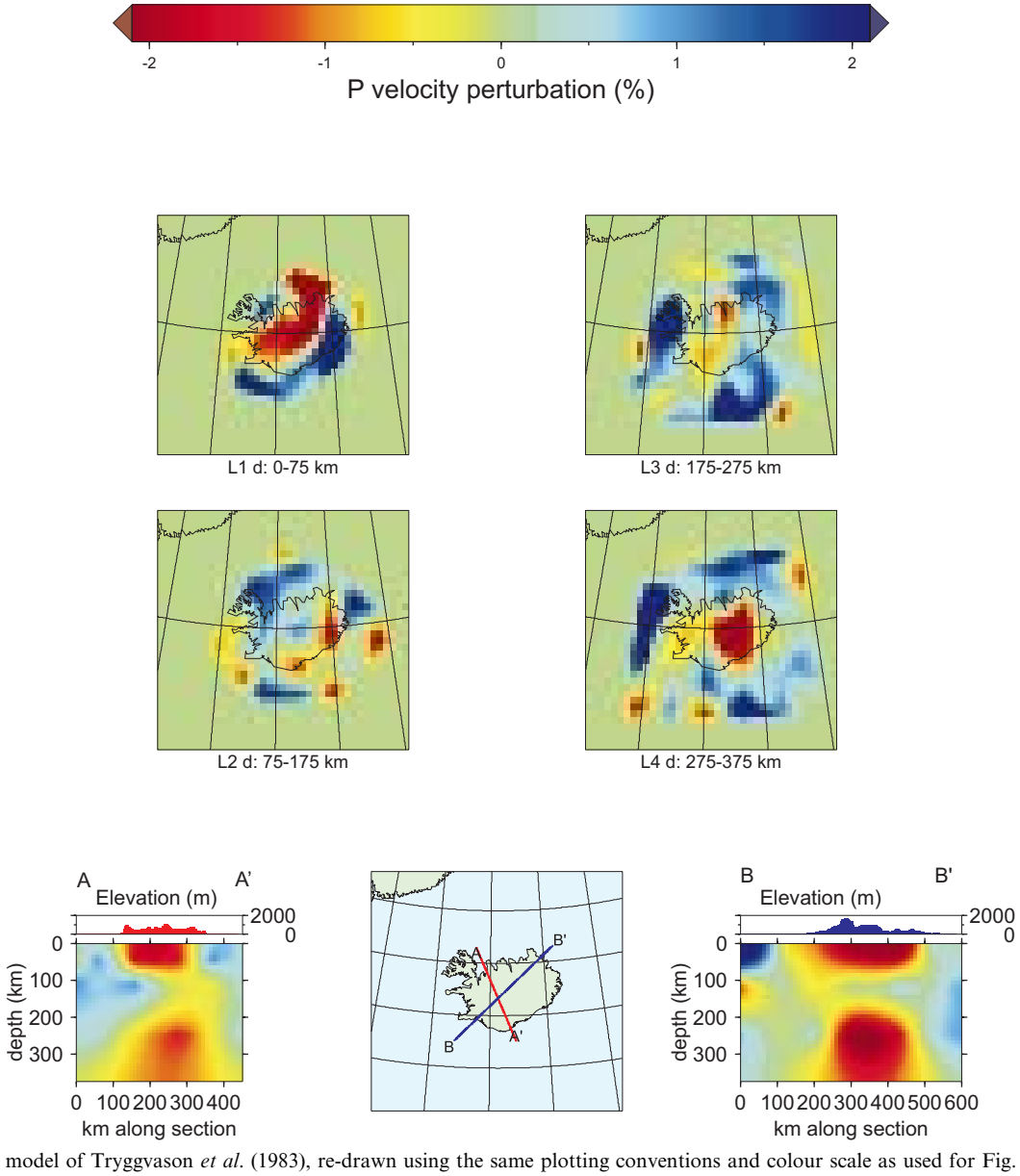

Figure 21. V_P model of Tryggvason *et al.* (1983), re-drawn using the same plotting conventions and colour scale as used for Fig. 13.

The dominant feature of both our study and that of Wolfe *et al.* (1997) is a negative wave-speed anomaly, with a diameter of about 200 km and strengths of up to 2–3 and 4–5 per cent in V_P and V_S, extending continuously to a depth of at least 400 km. The anomalies imaged by Wolfe *et al.* (1997) differ from ours in widening with depth in all directions. Keller *et al.* (2000) pointed out that the shape of the anomaly of Wolfe *et al.* (1997) closely resembles that of the incoming ray bundle, and questioned the resolution of the model at depths greater than about 200 km. They argued that the experiment cannot resolve structure deeper than $\sim$200 km, and that structure imaged below this depth could simply result from the downward smearing of shallow anomalies. The anomaly in our model also widens with depth in the north–south direction, but narrows in the east–west direction. By virtue of our wider array aperture, denser station distribution and larger and more diverse data set, our resolution is superior at all depths. The criticisms of Keller *et al.* (2000) are thus probably valid, and the east–west widening of the anomaly of Wolfe *et al.* (1997) is artificial. Clearly, the problem of resolution is of critical importance to using teleseismic tomography to seek plume-like structures because this type of experiment is prone to systematic distortions that can produce artificial anomalies of precisely the kind being sought.

Although Wolfe *et al.* (1997) did not point it out, except for V_P around 125 km, the anomaly in their model is centred on the eastern MVZ as it is in our model. Some tendency is also discernible for their anomaly, especially for V_P, to be elongated in the NNW direction at depths of about 300 km, in agreement with the systematic morphological change that we find. Wolfe *et al.* (1997) also found a positive V_P/V_S anomaly of up to $\sim +2$ per cent, which agrees with our result. The sparseness of the network used by Wolfe *et al.* (1997) resulted in a lack of crossing rays in the upper $\sim$100 km and a lack of resolution beneath the near-shore Reykjanes ridge. Thus neither the high wave speeds we image beneath the TFZ at shallow depths

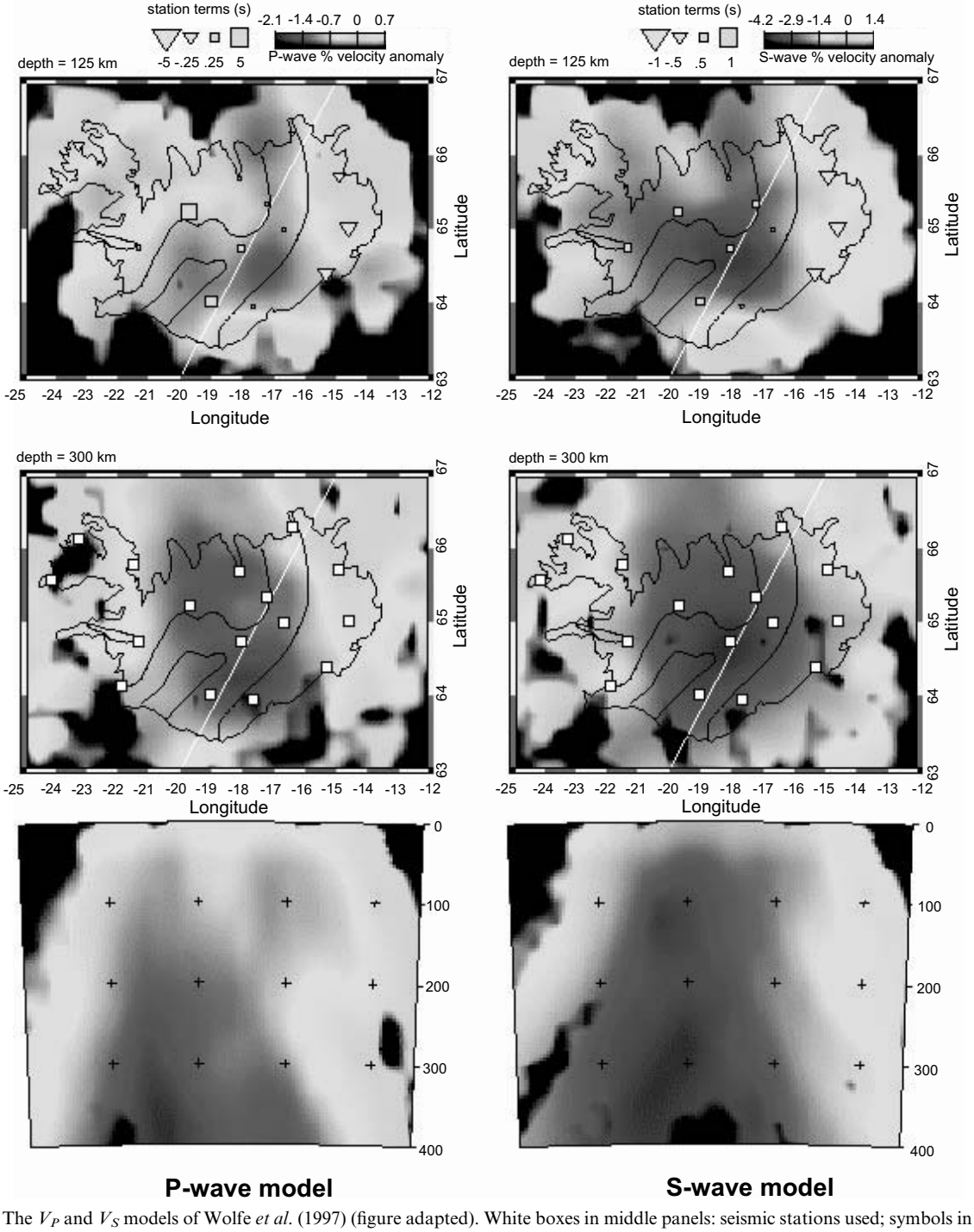

Figure 22. The V_P and V_S models of Wolfe *et al.* (1997) (figure adapted). White boxes in middle panels: seismic stations used; symbols in top panels: wave-speed perturbations in the 'special first layer'.

nor the low wave speeds beneath the Reykjanes ridge can be confirmed by that experiment.

Concluding remarks

Our results suggest that:

(i) central Iceland is underlain by a low-wave-speed anomaly consistent with a temperature anomaly of less than 200 K, whose width is 200–250 km and which extends to at least 450 km depth;

(ii) this anomaly is centred beneath the eastern MVZ rather than Vatnajokull;

(iii) low-degree partial melting is extensive beneath Iceland in the upper $\sim$300 km;

(iv) material rising beneath Iceland flows along the Reykjanes ridge but is blocked beneath the TFZ in the upper 100–200 km;

(v) the morphology of the anomaly changes from roughly cylindrical to tabular below about 250 km depth, in the manner expected for an upwelling from the transition zone, induced either by buoyancy or by passive upwelling; and

(vi) these observations are consistent with models that imply that the volcanic province currently associated with Iceland has been centred in the middle of the north Atlantic since its inception at ~54 Ma, and is thus not fixed relative to other Atlantic hotspots.

None of the tomography images currently available requires convective upwelling from the lower mantle beneath Iceland. The simplest model consistent with currently existing seismic data thus does not require a lower mantle plume, and the added constraint we have provided in the morphology of the anomaly is more consistent with a no-plume than a plume model. Alternative hypotheses should be considered to theories whose essential features lack observational support.

Some observations are consistent with a plume originating in the lower mantle. The thickness of the transition zone (that is, the separation of the 400 and 650 km discontinuities) is smaller beneath south Iceland than the global average. This is consistent with elevated temperatures, and Shen *et al.* (1998, 2001) interpreted it as evidence for a plume rising from the lower mantle. However, similar thickness variations have been detected elsewhere and there is no global correlation between these variations and hotspots (e.g. Chevrot *et al.* 1999), although this might be explained by a lack of resolution in the global studies. Ultra-low-wave-speed anomalies have been detected in a dome-shaped volume 250 km wide and 40 km high in region D″ just above the core–mantle boundary southwest of Iceland and interpreted as a partial melt body that could be the source of a lower mantle plume beneath Iceland (Helmberger *et al.* 1998). However, this anomaly may have nothing to do with the Iceland volcanic province, because region D″ is exceptionally heterogeneous everywhere and evidence for structural connection with the surface is absent. Observations of seismic anomalies for waves passing beneath the Iceland region and arriving at the Norwegian Seismic Array (NORSAR) are consistent with a weak negative V_P anomaly beneath the Iceland–Faeroes ridge, similar to that found by Bijwaard & Spakman (1999), but this interpretation is highly non-unique (Pritchard *et al.* 2000). The NORSAR data do not support an extension into the mid-lower mantle of the broader plume hypothesized by Shen *et al.* (1998, 2001) to underlie Iceland.

Much of the seismic evidence for a plume in the lower mantle beneath Iceland consists of observations of types that either are found elsewhere unaccompanied by hotspots or are not found beneath known hotspots. Many studies specifically seek a narrow, vertical, cylindrical body with a relatively strong anomaly, and the results tend to be interpreted in these terms if possible, although the observations may be consistent with other hypotheses.

Non-seismic data interpreted in support of plumes in the lower mantle include the broad geoid highs associated with hotspots, which indicate major low-density anomalies in the lower mantle (Richards & Hager 1988). Global surface heat flow requires the extraction of heat from the lower mantle and core (Davies 1988; Sleep 1990). Trace element and isotopic anomalies have been attributed variously to lower mantle plumes, the upper mantle or upper mantle sources with entrained lower mantle material (e.g. Fitton *et al.* 1997). In particular, high $^3He/^4He$ isotope ratios in some hotspot rocks (e.g. Hilton *et al.* 1999) are commonly attributed to excess ^3He from a primordial, little-degassed lower mantle (e.g. O'Nions & Tolstikhin 1994). This theory has recently been brought into question, however, and instead these observations may reflect an upper mantle source depleted in ^4He (e.g. Anderson 1998c,b; Graham *et al.* 1998; Foulger & Pearson 2001).

The deep structure beneath hotspots varies greatly. The East African rift is underlain by a strong negative V_P anomaly that plunges to the southwest, is ~2000 km wide and extends throughout the whole mantle to the core–mantle boundary (Woodhouse & Dziewonski 1984; Ritsema *et al.* 1999). This contrasts radically with the Iceland hotspot, where the strong seismic anomaly is confined to the upper mantle. Where clear, low-wave-speed, lower mantle bodies are detected by full-thickness mantle tomography beneath surface hotspots, they are far from having classical plume morphology. The simplistic model of tall, narrow, relatively simple, vertical, cylindrical pipe-like structures delivering hot material from deep within the lower mantle, or even transporting material within the upper mantle to the surface, is gaining little observational support, while that of shallow-seated phenomena is becoming increasingly viable.

ACKNOWLEDGMENTS

We are indebted to Jeroen Ritsema, Barbara Romanowicz, Charles Megnin, Rob van der Hilst and Hrafnkell Karason, who generously provided cross-sections through their mantle tomography models in the Iceland region (Figs 17, 18 and 19). This research was funded by Natural Environment Research Council (NERC) grants GST/02/1238 and GR3/10727, and NSF grant EAR 9417918. We thank the IRIS–PASSCAL instrument centre for lending the field equipment and providing technical assistance. MJP was supported by NERC studentship GT4/95/76E. Careful and painstaking reviews by R. van der Hilst, who straightened some of us out on whole-mantle tomography, and an anonymous reviewer greatly improved the manuscript. We were enlightened by discussions with D. L. Anderson.

REFERENCES

Aki, K., Christoffersson, A. & Husebye, E., 1977. Determination of the three-dimensional seismic structure of the lithosphere, *J. geophys. Res.,* **82,** 277–296.

Allen, R.M. *et al.*, 1999. The thin hot plume beneath Iceland, *Geophys. J. Int.,* **137,** 51–63.

Anderson, D.L., 1989. *Theory of the Earth,* Blackwell Scientific Publications, Boston.

Anderson, D.L., 1998a. The EDGES of the mantle, in *The Core–Mantle Boundary Region*, pp. 255–271, eds Gurnis, M.E., Wysession, E.K. & Buffett, B.A., AGU, Washington, DC.

Anderson, D.L., 1998b. The helium paradoxes, *Proc. Nat. Acad. Sci.,* **95,** 4822–4827.

Anderson, D.L., 1998c. A model to explain the various paradoxes associated with mantle noble gas geochemistry, *Proc. Nat. Acad. Sci.,* **95,** 9087–9092.

Anderson, D.L. & Bass, J.D., 1984. Mineralogy and composition of the upper mantle, *Geophys. Res. Lett.,* **11,** 637–640.

Anderson, D.L. & Sammis, C., 1970. Partial melting in the upper mantle, *Phys. Earth planet. Inter.,* **3,** 41–50.

Bernauer, F., 1943. Junge Tektonik Auf Island und Ihre Ursachen, in *Spalten Auf Island—Geologische, Geodaetische und Geophysikalische Forschungsarbeiten der Deutschen Island-Expedition Des Jahres 1938,* ed. Niemczyk, O., Verlag von Konrad Wittwer, Stuttgart.

Bijwaard, H. & Spakman, W., 1999. Tomographic evidence for a narrow whole mantle plume below Iceland, *Earth planet. Sci. Lett.,* **166,** 121–126.

Bjarnason, I.T., Wolfe, C.J., Solomon, S.C. & Gudmundson, G., 1996. Initial results from the ICEMELT experiment: body-wave delay times and shear-wave splitting across Iceland, *Geophys. Res. Lett.,* **23,** 459–462.

Bott, M.H.P., 1985. Plate tectonic evolution of the Icelandic transverse ridge and adjacent regions, *J. geophys. Res.,* **90,** 9953–9960.

Chevrot, S., Vinnik, L. & Montagner, J.P., 1999. Global-scale analysis of the mantle *Pds* phases, *J. geophys. Res.,* **104,** 20 203–20 219.

Darbyshire, F.A., Bjarnason, I.T., White, R.S. & Flovenz, O.G., 1998. Crustal structure above the Iceland mantle plume imaged by the ICEMELT refraction profile, *Geophys. J. Int.,* **135,** 1131–1149.

Davies, G.F., 1988. Ocean bathymetry and mantle convection 1, Large-scale flow and hotspots, *J. geophys. Res.,* **93,** 10 467–10 480.

Du, Z.J. & Foulger, G.R., 1999. The crustal structure beneath the Northwest Fjords, Iceland, from receiver functions and surface waves, *Geophys. J. Int.,* **139,** 419–432.

Du, Z. & Foulger, G.R., 2001. Variation in the crustal structure across central Iceland, *Geophys. J. Int.,* **145,** 246–264.

Du, Z. *et al.*, 2001. Crustal structure beneath western and eastern Iceland from surface waves and receiver functions, *Geophys. J. Int.*, submitted.

Engdahl, E.R., van der Hilst, R.D. & Buland, R.P., 1998. Global teleseismic earthquake relocation from improved travel times and procedures for depth determination, *Bull. seism. Soc. Am.,* **88,** 722–743.

Evans, J.R. & Achauer, U., 1993. Teleseismic velocity tomography using the ACH method: theory and application to continental-scale studies, in *Seismic Tomography: Theory and Applications*, pp. 319–360, eds Iyer, H.M. & Hirahara, K., Chapman & Hall, London.

Faul, U.H., Toomey, D.R. & Waff, H.S., 1994. Intergranular basaltic melt is distributed in thin, elongated inclusions, *Geophys. Res. Lett.,* **21,** 29–32.

Feighner, M.A. & Kellogg, L.H., 1995. Numerical modeling of chemically buoyant mantle plumes at spreading ridges, *Geophys. Res. Lett.,* **22,** 715–718.

Fitton, J.G., Saunders, A.D., Norry, M.J., Hardarson, B.S. & Taylor, R.N., 1997. Thermal and chemical structure of the Iceland plume, *Earth planet. Sci. Lett.,* **153,** 197–208.

Foulger, G.R. & Pearson, D.G., 2001. Is Iceland underlain by a plume in the lower mantle? Seismology and helium isotopes, *Geophys. J. Int.,* **145,** F1–F5.

Foulger, G.R. *et al.*, 2000. The seismic anomaly beneath Iceland extends down to the mantle transition zone and no deeper, *Geophys. J. Int.,* **142,** F1–F5.

Fukao, Y., Obayashi, M., Inoue, H. & Nenbai, M., 1992. Subducting slabs stagnate in the mantle transition zone, *J. geophys. Res.,* **97,** 4809–4822.

Goes, S., Govers, R. & Vacher, P., 2000. Shallow mantle temperatures under Europe from *P* and *S* wave tomography, *J. geophys. Res.,* **105,** 11 153–11 169.

Graham, D.W., Larsen, L.M., Hanan, B.B., Storey, M., Pedersen, A.K. & Lupton, J.E., 1998. Helium isotope composition of the early Iceland mantle plume inferred from Tertiary picrites of west Greenland, *Earth planet. Sci. Lett.,* **160,** 241–255.

Grand, S.P., 1994. Mantle shear structure beneath the Americas and surrounding oceans, *J. geophys. Res.,* **99,** 11 591–11 621.

Gudmundsson, M.T., Sigmundsson, F. & Bjornsson, H., 1997. Ice–volcano interaction of the 1996 Gjalp subglacial eruption, Vatnajokull, Iceland, *Nature,* **389,** 954–957.

Gutenberg, B., 1959. The asthenosphere low-velocity layer, *Ann. Geofis.,* **12,** 439–460.

Hager, B.H. & Clayton, R.W., 1989. Constraints on the structure of mantle convection using seismic observations, flow models, and the geoid, in *Mantle Convection, Plate Tectonics and Global Dynamics*, pp. 657–764, ed. Peltier, W.R., Gordon & Breach, New York.

Halbert, S.E., Buland, R. & Hutt, C.R., 1988. *Standard for the Exchange of Earthquake Data (SEED)*, Version V2.0, USGS, Albuquerque Seismological Laboratory, NM.

Harvey, D. & Quinlan, D., 1996. *Datascope Seismic Application Package (DSAP), Rept Joint Seismic Processing Center,* University of Colorado, CO.

Helmberger, D.V., Wen, L. & Ding, X., 1998. Seismic evidence that the source of the Iceland hotspot lies at the core–mantle boundary, *Nature,* **396,** 251–255.

Hilton, D.R., Gronvold, K., Macpherson, C.G. & Castillo, P.R., 1999. Extreme $^{3}He/^{4}He$ ratios in northwest Iceland: constraining the common component in mantle plumes, *Earth planet. Sci. Lett.,* **173,** 53–60.

Holmes, A., 1931. Radioactvity and Earth movements, *Trans. geol. Soc. Glasgow 1928–29,* **18,** 559–606.

Houseman, G.A., 1990. The thermal structure of mantle plumes: axisymmetric or triple-junction?, *Geophys. J. Int.,* **102,** 15–24.

Ito, G., Lin, J. & Gable, C.W., 1996. Dynamics of mantle flow and melting at a ridge-centered hotspot: Iceland and the mid-Atlantic ridge, *Earth planet. Sci. Lett.,* **144,** 53–74.

Iwamori, H., McKenzie, D. & Takahashi, E., 1995. Melt generation by isentropic mantle upwelling, *Earth planet. Sci. Lett.,* **134,** 253–266.

Julian, B.R., Evans, J.R., Pritchard, M.J. & Foulger, G.R., 2001. A geometrical error in some versions of the ACH method of teleseismic tomography, *Bull. seism. Soc. Am.,* **90,** 1554–1558.

Karason, H. & van der Hilst, R.D., 2001a. Tomographic imaging of the lowermost mantle with differential times of refracted and diffracted core phases (*PKP, P_{diff}*), *J. geophys. Res.,* **106,** 6569–6587.

Karason, H. & van der Hilst, R.D., 2001b. Mantle P-wave speed from seismic tomography: advances in methodology and data integration, *J. geophys. Res.,* submitted.

Karato, S., 1993. Importance of anelasticity in the interpretation of seismic tomography, *Geophys. Res. Lett.,* **20,** 1623–1626.

Keller, W.R., Anderson, D.L. & Clayton, R.W., 2000. Difficulties in seismically imaging the Icelandic hotspot, *Geophys. Res. Lett.,* **27,** 3993–3996.

Kendall, J.-M., 1994. Teleseismic arrivals at a mid-ocean ridge: effects of mantle melt and anisotropy, *Geophys. Res. Lett.,* **21,** 301–304.

Kennett, B.L.N. & Engdahl, E.R., 1991. Travel times for global earthquake location and phase identification, *Geophys. J. Int.,* **105,** 429–466.

King, S.D. & Anderson, D.L., 1995. An alternative mechanism of flood basalt formation, *Earth planet. Sci. Lett.,* **136,** 269–279.

King, S.D. & Anderson, D.L., 1998. Edge-driven convection, *Earth planet. Sci. Lett.,* **160,** 289–296.

Korenaga, J., 2000. Magmatism and dynamics of continental breakup in the presence of a mantle plume, *PhD thesis,* MIT, Cambridge, MA.

McKenzie, D. & Bickle, M.J., 1988. The volume and composition of melt generated by extension of the lithosphere, *J. Petrol.,* **29,** 625–679.

Megnin, C. & Romanowicz, B., 1998. The effect of theoretical formalism and data selection scheme on mantle models derived from waveform tomography, *Geophys. J. Int.,* **138,** 366–380.

Megnin, C. & Romanowicz, B., 2000. The three-dimensional velocity structure of the mantle from the inversion of body, surface and higher-mode waveforms, *Geophys. J. Int.,* **143,** 709–728.

Morgan, W.J., 1971. Convection plumes in the lower mantle, *Nature,* **230,** 42–43.

Morgan, W.J., 1972. Plate motions and deep mantle convection, *Geol. Soc. Am. Bull.,* **132,** 7–22.

O'Nions, R.K. & Tolstikhin, I.N., 1994. Behaviour and residence times of lithophile and rare gas tracers in the upper mantle, *Earth planet. Sci. Lett.,* **124,** 131–138.

Pritchard, M.J., 2000. A seismological study of the mantle beneath Iceland, *PhD thesis,* University of Durham, Durham.

Pritchard, M.J., Foulger, G.R., Julian, B.R. & Fyen, J., 2000. Constraints on a plume in the mid-mantle beneath the Iceland region from seismic-array data, *Geophys. J. Int.,* **143,** 119–128.

Ramberg, H., 1981. *Gravity, Deformation and the Earth's Crust,* Academic Press, London.

Ribe, N.M., Christensen, U.R. & Theissing, J., 1995. The dynamics of plume–ridge interaction, 1: Ridge-centered plumes, *Earth planet. Sci. Lett.,* **134,** 155–168.

Richards, M.A. & Hager, B.H., 1988. Dynamically supported geoid highs over hotspots: observations and theory, *J. geophys. Res.,* **93,** 7690–7708.

Ritsema, J., van Heijst, H.J. & Woodhouse, J.H., 1999. Complex shear wave velocity structure imaged beneath Africa and Iceland, *Science,* **286,** 1925–1928.

Saemundsson, K., 1979. Outline of the geology of Iceland, *Jokull,* **29,** 7–28.

Saemundsson, K., Kristjansson, L., McDougall, I. & Watkins, N.D., 1980. K-Ar dating, geological and paleomagnetic study of a 5-km lava succession in northern Iceland, *J. geophys. Res.,* **85,** 3628–3646.

Schilling, J.-G., 1973. Iceland mantle plume: geochemical study of Reykjanes ridge, *Nature,* **242,** 565–571.

Schilling, J.-G., 1991. Fluxes and excess temperatures of mantle plumes inferred from their interaction with migrating mid-ocean ridges, *Nature,* **352,** 397–403.

Schilling, J.-G., Thompson, G., Kingsley, R. & Humphris, S., 1985. Hotspot–migrating ridge interaction in the south Atlantic, *Nature,* **313,** 187–191.

Schmeling, H., 2000. Partial melting and melt segregation in a convecting mantle, in *Physics and Chemistry of Partially Molten Rocks,* pp. 141–178, eds Bagdassarov, N., Laporte, D. & Thompson, A.B., Kluwer, Dordrecht.

Shen, Y. & Forsyth, D.W., 1995. Geochemical constraints on initial and final depths of melting beneath mid-ocean ridges, *J. geophys. Res.,* **100,** 2211–2237.

Shen, Y., Solomon, S.C., Bjarnason, I.T. & Wolfe, C.J., 1998. Seismic evidence for a lower-mantle origin of the Iceland plume, *Nature,* **395,** 62–65.

Shen, Y. *et al.*, 2001. Seismic evidence for a tilted mantle plume and north–south mantle flow beneath Iceland, *Science,* submitted.

Sigmundsson, F., Einarsson, P., Bilham, R. & Sturkell, E., 1994. Rift-transform kinematics in south Iceland: deformation from GPS measurements 1986–1992, *J. geophys. Res.,* **100,** 6235–6248.

Sigvaldason, G.E., Steinthorsson, S., Oskarsson, N. & Imsland, P., 1974. Compositional variation in recent Icelandic tholeiites and the Kverkfjoll hot spot, *Nature,* **251,** 579–582.

Sleep, N.H., 1990. Hotspots and mantle plumes: some phenomenology, *J. geophys. Res.,* **95,** 6715–6736.

Sleep, N.H., 1996. Lateral flow of hot plume material ponded at sublithospheric depths, *J. geophys. Res.,* **101,** 28 065–28 083.

Sleep, N.H., 1997. Lateral flow and ponding of starting plume material, *J. geophys. Res.,* **102,** 10 001–10 012.

Spetzler, H. & Anderson, D.L., 1968. The effect of temperature and partial melting on velocity and attenuation in a simple binary system, *J. geophys. Res.,* **73,** 6051–6060.

Steck, L.K. & Prothero, W.A., 1991. A 3-D raytracer for teleseismic body-wave arrival times, *Bull. seism. Soc. Am.,* **81,** 1332–1339.

Stefánsson, R. *et al.*, 1993. Earthquake prediction research in the south Iceland seismic zone and the SIL project, *Bull. seism. Soc. Am.,* **83,** 696–716.

Tackley, P.J., 1998. Self-consistent generation of tectonic plates in three-dimensional mantle convection, *Earth planet. Sci. Lett.,* **157,** 9–22.

Thorbergsson, G., Magnusson, I.T. & Palmason, G., 1990. *Gravity Data and Gravity Map of Iceland,* Rept OS-90001/JHD-01, National Energy Authority, Reykjavik.

Tryggvason, K., Husebye, E.S. & Stefánsson, R., 1983. Seismic image of the hypothesized Icelandic hot spot, *Tectonophysics,* **100,** 94–118.

van der Hilst, R. & Karason, H., 1999. Compositional heterogeneity in the bottom 1000 kilometers of Earth's mantle: toward a hybrid convection model, *Science,* **283,** 1885–1888.

van der Hilst, R., Widiyantoro, S. & Engdahl, E.R., 1997. Evidence for deep mantle circulation from global tomography, *Nature,* **353,** 37–42.

Vink, G.E., 1984. A hotspot model for Iceland and the Voring Plateau, *J. geophys. Res.,* **89,** 9949–9959.

Vogt, P.R., 1976. Plumes, sub-axial pipe flow, and topography along mid-oceanic ridges, *Earth planet. Sci. Lett.,* **29,** 309–325.

White, R.S. & McKenzie, D.P., 1995. Mantle plumes and flood basalts, *J. geophys. Res.,* **100,** 17 543–17 585.

White, R.S., Bown, J.W. & Smallwood, J.R., 1995. The temperature of the Iceland plume and origin of outward-propagating V-shaped ridges, *J. Geol. Soc. Lond.,* **152,** 1039–1045.

Wilson, J.T., 1963. A possible origin of the Hawaiian Islands, *Can. J. Phys.,* **41,** 863–870.

Wolfe, C.J., Bjarnason, I.T., VanDecar, J.C. & Solomon, S.C., 1997. Seismic structure of the Iceland mantle plume, *Nature,* **385,** 245–247.

Woodhouse, J.H. & Dziewonski, A.M., 1984. Mapping the upper mantle—3-dimensional modeling of Earth structure by inversion of seismic waveforms, *J. geophys. Res.,* **89,** 5953–5984.

Zhou, H.W., 1996. A high resolution *P*-wave model for the top 1200 km of the mantle, *J. geophys. Res.,* **101,** 27 791–27 810.